Article

Immunity

Ambient oxygen levels regulate intestinal dysbiosis and GVHD severity after allogeneic stem cell transplantation

Graphical abstract

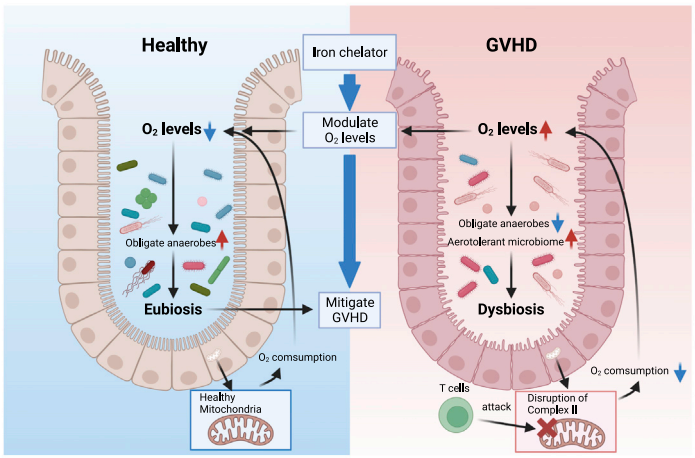

Highlights

- Allogeneic intestinal dysbiosis is not pathogenic to naive animals
- Loss of intestinal physiologic hypoxia causes dysbiosis
- The defect in oxygen utilization in IECs leads to a loss of intestinal hypoxia
- Oxygen modulation after allo-HSCT improves intestinal hypoxia and GVHD

Authors

Keisuke Seike, Anders Kiledal, Hideaki Fujiwara, ..., Robert R. Jenq, Gregory Dick, Pavan Reddy

Correspondence

pavan.reddy@bcm.edu

In brief

Whether dysbiosis is a cause or consequence of pathology in intestinal diseases is not understood. Here, Seike et al. show that defective oxygen utilization by intestinal epithelial cells leads to a loss of intestinal hypoxia and concomitant dysbiosis. Oxygen modulation rescues intestinal hypoxia and alleviates gastrointestinal graft-versus-host disease.

Seike et al., 2023, Immunity *56*, 353–368
February 14, 2023
https://doi.org/10.1016/j.immuni.2023.01.007

CellPress

Immunity

CellPress

Article

Ambient oxygen levels regulate intestinal dysbiosis and GVHD severity after allogeneic stem cell transplantation

Keisuke Seike,[1,12] Anders Kiledal,[2,12] Hideaki Fujiwara,[3,12] Israel Henig,[4,12] Marina Burgos da Silva,[5,12] Marcel R.M. van den Brink,[5] Robert Hein,[2] Matthew Hoostal,[6] Chen Liu,[7] Katherine Oravecz-Wilson,[1] Emma Lauder,[1] Lu Li,[1] Yaping Sun,[1] Thomas M. Schmidt,[6] Yatrik M. Shah,[8,9] Robert R. Jenq,[10] Gregory Dick,[2] and Pavan Reddy[1,11,13,*]

[1]Department of Internal Medicine, Division of Hematology and Oncology, University of Michigan, Rogel Cancer Center, Ann Arbor, MI, USA
[2]Department of Earth & Environmental Sciences, University of Michigan, Ann Arbor, MI 48109, USA
[3]Department of Hematology and Oncology, Okayama University Hospital, 2-5-1, Shikata-cho, Kita-ku, Okayama 700-8558, Japan
[4]Department of Hematology, Rambam Health Care Campus, Haifa, Israel
[5]Department of Immunology, Sloan Kettering Institute, Memorial Sloan Kettering Cancer Center, New York, NY 10065, USA
[6]Department of Internal Medicine, Division of Infectious Disease, University of Michigan Health System, Ann Arbor, MI, USA
[7]Department of Pathology, Yale University School of Medicine, New Haven, CT, USA
[8]Department of Internal Medicine, Division of Gastroenterology, University of Michigan Health System, Ann Arbor, MI, USA
[9]Department of Molecular and Integrative Physiology, University of Michigan School of Medicine, Ann Arbor, MI, USA
[10]Department of Genomic Medicine, Division of Cancer Medicine, MD Anderson Cancer Center, Houston, TX, USA
[11]Dan L Duncan Comprehensive Cancer Center, Baylor College of Medicine, Houston, TX, USA
[12]These authors contributed equally
[13]Lead contact
*Correspondence: pavan.reddy@bcm.edu
https://doi.org/10.1016/j.immuni.2023.01.007

SUMMARY

The severity of T cell-mediated gastrointestinal (GI) diseases such as graft-versus-host disease (GVHD) and inflammatory bowel diseases correlates with a decrease in the diversity of the host gut microbiome composition characterized by loss of obligate anaerobic commensals. The mechanisms underpinning these changes in the microbial structure remain unknown. Here, we show in multiple specific pathogen-free (SPF), gnotobiotic, and germ-free murine models of GI GVHD that the initiation of the intestinal damage by the pathogenic T cells altered ambient oxygen levels in the GI tract and caused dysbiosis. The change in oxygen levels contributed to the severity of intestinal pathology in a host intestinal HIF-1α- and a microbiome-dependent manner. Regulation of intestinal ambient oxygen levels with oral iron chelation mitigated dysbiosis and reduced the severity of the GI GVHD. Thus, targeting ambient intestinal oxygen levels may represent a novel, non-immunosuppressive strategy to mitigate T cell-driven intestinal diseases.

INTRODUCTION

The composition of host intestinal microbiome directly contributes to human health and diseases. Correspondingly, a healthy gut is inhabited by a diverse community of mostly obligate anaerobic bacteria (eubiosis) that is influenced by the host genetics, diet, and immunity.[1,2] The breakdown of this balance, called dysbiosis and often characterized by a shift in the microbial community structure from obligate to facultative anaerobes and aerotolerant microbes, is associated with several diseases, including immune-mediated intestinal diseases such as graft-versus-host disease (GVHD).[3–6] While a strong correlation exists between disease severity and dysbiosis, the mechanisms that lead to dysbiosis are unknown. Furthermore, whether dysbiosis is a cause, an amplifier, a regulator, or a mere consequence of the disease process remains poorly understood.

Gastrointestinal (GI) GVHD is a potentially fatal complication of allogeneic hematopoietic stem cell transplantation (allo-HSCT).[7] Reduction in intestinal microbial diversity with loss of obligate anaerobes relative to other bacteria is associated with increased GVHD mortality.[3,8,9] However, seminal experimental studies performed before the advent of modern germ-free (GF) facilities and sequencing technologies demonstrated that absence of microbiome mitigated GVHD severity.[10] Thus, while microbial dysbiosis prognosticates outcomes after allo-HSCT, the role of microbiome in GVHD remains unclear. Specifically, (1) whether dysbiosis is caused by or is a consequence of severe GVHD, (2) the mechanisms that underpin the development of dysbiosis, and (3) whether dysbiosis before or after HSCT directly amplifies or negatively regulates GVHD severity remain unknown.

The mammalian GI tract is hypoxic with an oxygen (O_2) gradient that traverses the surface of the colonic mucosa to

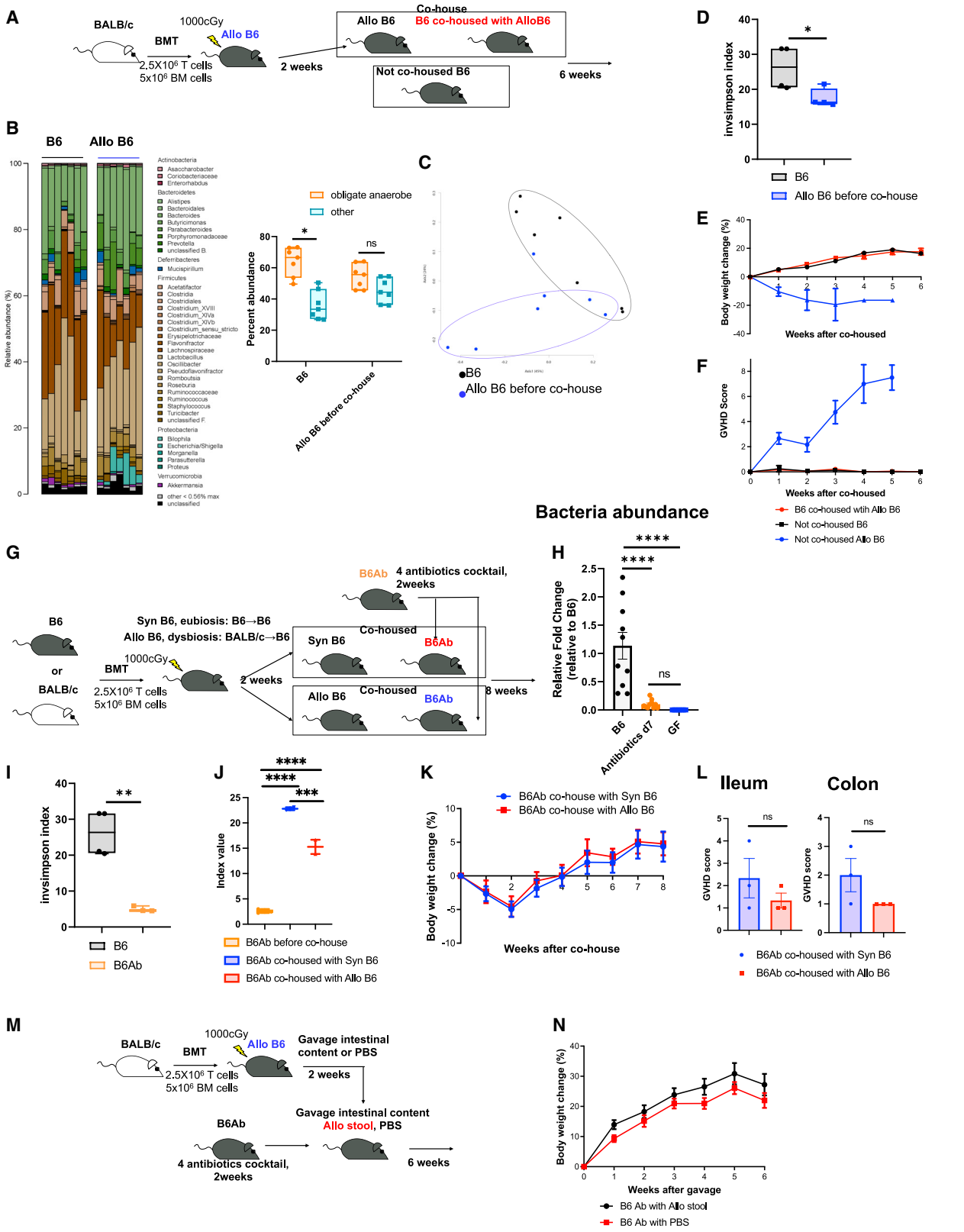

Figure 1. Allogeneic dysbiosis is not pathogenic to naive animals

(A–F) Naive C57BL/6 mice (B6) 7–8 weeks old were cohoused with allogeneic recipient mice (Allo B6) 2 weeks after post-transplant.

(A) Mice were cohoused in a ratio of 1:1 naive mice to BMT mice, respectively. Data are from 3 independent experiments (N = 9). Stool from from Allo B6 before co-house or B6 were analyzed by 16S rRNA gene sequencing.

(legend continued on next page)

the center of gut lumen. This hypoxic gradient shapes the intestinal microbial community structure, promoting colonization with predominantly obligate anaerobes at homeostasis.[11,12] The host intestinal epithelial cells (IECs) are thus uniquely adapted to the hypoxic environment, i.e., "physiologic hypoxia." The IECs depend on microbial metabolites, specifically short-chain fatty acids (SCFAs), as their primary source of energy for oxidative phosphorylation (OXPHOS) despite low oxygen.[13,14] Thus, microbial-derived SCFAs regulate the barrier function at homoeostasis[15] and in GI GVHD.[16,17] Moreover, epithelial metabolism and the cellular O_2 sensor, hypoxia-inducible factor 1α (HIF-1α), are key determinants of intestinal function under conditions of physiologic hypoxia.[1,18] In the context of enteric infections, intestinal ambient oxygen level is a critical ecological driver of dysbiosis.[1,2,19,20] In the context of non-infectious immune-mediated GI damage, pathogenic T cells target OXPHOS in the IEC leading to deficient O_2 utilization.[21] However, whether the change in the luminal oxygen due to poor consumption of O_2 from the metabolic defect impacts dysbiosis remains unknown.

Herein, we showed that dysbiosis was a consequence of the loss of "physiologic hypoxia" caused by poor oxygen utilization by the IECs.[21] We also showed that the microbiome by itself is a critical negative regulator of GI GVHD. In contrast to the current paradigm, GF animals demonstrated greater GVHD while promotion of eubiosis "after" transplant mitigated the severity of GVHD. However, dysbiosis "before" HSCT did not impact GVHD severity. Rescue of physiological hypoxia by iron chelation mitigated the severity of GI GVHD. Thus, our data provide a mechanism for induction of dysbiosis and demonstrate that promotion of eubiosis by regulating ambient oxygen reduces the severity of intestinal damage after allo-HCT.

RESULTS

Allogeneic dysbiosis is not pathogenic to naive animals

We first determined whether dysbiosis associated with GVHD following allogeneic HSCT is toxic in the absence of HSCT. Naive C57BL/6 (B6) animals were irradiated with 10 Gy and transplanted with splenic T cells and T cell-depleted bone marrow (TCD BM) from allogeneic BALB/c donors (Allo B6) to induce GVHD and dysbiosis (Figure 1A). Dysbiosis in stool from Allo B6 animals was confirmed at 2 weeks (Figures 1B–1D, S1A, and S1B). Allo B6 stools contained more Proteobacteria, particularly facultative anaerobes in the Enterobacteriaceae family such as *Escherichia* (Figures 1A and 1B). Allo B6 animals were cohoused with a cohort of naive, un-transplanted B6 hosts for 6 weeks (B6 cohoused with Allo B6), while a cohort of naive B6 animals from the same colony were not cohoused (not cohoused B6) and served as control animals (see Figure 1A). Microbiomes of B6 cohoused with Allo B6 changed toward Allo B6 at 6 weeks (Figures S1C–S1G). Despite the shift in community structure and reduction in diversity, both the cohoused and non-cohoused cohorts of un-transplanted naive B6 mice showed similar weight gain with no signs of GVHD (Figures 1E and 1F).

It is possible that some organisms in the endogenous normal microbiome of the cohoused mice may have prevented the pathogenic effects of dysbiosis. Therefore, we examined the impact of dysbiosis in naive B6 animals treated with a cocktail of four antibiotics to effectively clear endogenous GI microbiome in B6 hosts.[3] The naive B6 animals were treated with the four-antibiotic cocktail for 2 weeks (B6Ab, Figure 1G), and near-complete loss of microbiome was confirmed (Figures 1H, 1I, S2A, and S2B) before cohousing with Allo B6 as above. To further control for the ability of microbiota from transplanted mice to colonize naive antibiotic-treated B6 hosts, we also cohoused another cohort of these animals with B6 syngeneic bone marrow transplantation (BMT) (Syn B6, Figure 1G). We confirmed that B6 and Syn B6 showed similar microbiome and eubiosis (Figures S2C and S2D). The naive, un-transplanted B6 animals were cohoused and monitored for 8 weeks for signs of weight loss and GI damage. Cohousing with Allo B6 caused dysbiosis (Figure 1J). As shown in Figures 1K and 1L, cohousing of the un-transplanted antibiotic-treated naive B6 hosts with either dysbiotic Allo B6 or the control Syn B6 animals did not impact weight gain or cause GVHD.

It is formally possible that cohousing alone might not be sufficient to cause complete microbiota alterations and cause

(B–D) Microbiome composition (left) with the percent abundance of obligate anaerobes and other bacteria (right) (B), PCoA (C), and inverse Simpson alpha diversity index of microbiome (D) in stool were shown.
(E and F) The body weight change (E) and the clinical GVHD score (F) of B6 cohoused with Allo B6, not cohoused B6, and not cohoused Allo B6 are shown (cohoused with Allo B6 and not cohoused B6: N = 9, not cohoused Allo B6; N = 6).
(G–L) B6 mice 6–8 weeks old were treated with 2 weeks of 4 antibiotics cocktail (ampicillin 1 gr/L, kanamycin 1 gr/L, metronidazole 1 gr/L, and vancomycin 0.5 gr/L plus 3% stevia) in filtered double distillated drinking water.
(G) Antibiotic-treated mice (B6Ab) were cohoused in ratio of 1:1 antibiotic-treated mice to BMT mice, respectively. Data are from 3 independent experiments.
(H) Stool from B6Ab, B6, and germ-free (GF) mice was analyzed by qPCR. Relative quantification of bacteria in stool from B6, antibiotics treated B6 at day 7, and GF mice were analyzed (B6: N = 10, antibiotics d7: N = 10, GF: N = 8).
(I) Inverse Simpson alpha diversity index of microbiome of B6 and B6Ab are shown (B6N: N = 4, B6Ab, N = 3).
(J) Inverse Simpson alpha diversity index of microbiome of B6Ab, B6Ab cohoused with Syn or Allo B6 at day 14 after co-house were shown (B6Ab N = 4, B6Ab cohoused with Syn or Allo B6 N = 2).
(K) The body weight changes of cohoused B6Ab mice are shown (cohoused with Syn: N = 14, cohoused with Allo: N = 15).
(L) Ileal and colonic histopathological GVHD score of cohoused B6Ab mice are shown (N = 3).
(M and N) B6 mice were treated for 2 weeks with 4 antibiotics cocktail (ampicillin 1 mg/mL, neomycin 1 mg/mL, metronidazole 1 mg/mL, and vancomycin 0.5 mg/mL) in filtered double distillated drinking water, followed by 10 doses of intestinal content gavage from BMT recipient mice 2 weeks after BMT. Each gavage day 1 BMT mouse whole gut content was collected. Stool solution was gavaged to each recipient mouse. (M) Data are from 3 independent experiments (B6Ab with allo-stool: N = 15, B6Ab with PBS: N = 8). (N) The body weight change of gavaged B6Ab mice are shown.
The horizontal line in box (B, D, I, and J) represents the median with the box bounding the interquartile range. The ends of the whisker lines represent the minimum and maximum values. Two-tailed paired Wilcoxon test (B) and two-tailed unpaired t test (D, I, and L), and one-way ANOVA analysis with Tukey post hoc test (H and J) were used to determine significance (mean ± SEM). *p < 0.05, **p < 0.01, ***p < 0.001, ****p < 0.0001.
See also Figures S1 and S2.

dysbiosis in un-transplanted naive B6 animals, despite pre-treatment with antibiotic cocktails. Therefore, to mitigate any potential inefficiencies of cohousing on changes to the microbiome, we treated the naive B6 un-transplanted hosts with the antibiotics or diluent control as above and then directly gavaged them with intestinal content from Allo B6 animals (Figure 1M) and monitored as above. Gavage of antibiotic-treated naive B6 animals with Allo B6 stools caused dysbiosis (Figures S2E and S2F). Un-transplanted antibiotic-treated naive B6 animals that received dysbiotic stool gavage from Allo B6 animals showed similar body weight gain as control un-transplanted antibiotic-treated naive B6 controls that received PBS gavage (Figure 1N).

While clinical features of GI damage were not apparent, it is possible that gavage of the dysbiotic stool into the antibiotic-treated, naive un-transplanted B6 mice might cause changes in host immunity. We therefore gavaged Allo B6 stool, the control Syn B6 stool, PBS, or sham into antibiotic-treated animals as above and performed systematic phenotyping of T cells (phenotype, cytokine, regulatory T [Treg] cells) and dendritic cells in distant secondary lymph nodes (LNs), spleen and regional (mesenteric) LNs on days 14 and 42 after the stool gavage (Figures S3A and S3B). No significant differences were noted the in the $CD4^+$ and $CD8^+$ subsets, PD1, CD69, CD62L, CD44, $CD4^+Foxp3^+$ Tregs, T cell IFNγ, IL-4 and IL-17A, or the CD80, CD86, 40, PDL1, IL-6, and TNF-α expression in the $CD11c^+$ cells) between the cohorts. Furthermore, the local tissue T cell phenotype (in colon and ileum) and numbers were also similar between all cohorts (Figure S3C).

When we analyzed histopathological changes in the small and large intestines that may have been caused by transfer of dysbiotic stool, we found no evidence of damage or significant differences between the groups at 2 weeks (Figure S3D) or 6 weeks (Figure S3E) after intestinal content gavage. These data collectively demonstrate that a shift toward dysbiosis did not affect the intestinal health of the un-transplanted naive B6 animals and that allo-dysbiosis by itself is not deleterious in the absence of preceding damage. Thus, dysbiosis after allo-HCT is not a cause, but is a consequence of GVHD.

Post-transplant but not pre-transplant dysbiosis regulates GVHD

We next addressed whether changes to the microbiome after allo-HCT influence GVHD severity. To this end, we explored whether host dysbiosis "before" transplant impacts GVHD outcomes. B6 animals were treated with either antibiotics or diluent controls and reconstituted with stool microbiome from Allo B6 animals (Figure 2A). They were then lethally irradiated (10 Gy) and transplanted with 5×10^6 BM cells and 2.5×10^6 splenic T cells from either B6 syngeneic or allogeneic BALB/donors. Allogeneic recipients with or without antibiotics and stool gavage showed dysbiosis and similar microbiome between allogeneic groups, but changes from B6 mice before HCT (Figures 2B and 2C). However, all of the allogeneic recipients with or without dysbiosis prior to the transplant showed similar mortality and clinical GVHD severity (Figures 2D and 2E). Histopathology of the intestine confirmed similar pathological GVHD severity (Figure 2F). These data suggest that the status of the pre-transplant microbiome does not substantially impact GVHD outcomes.

Pre-transplant dysbiosis does not address the issue of the impact of the change from pre-BMT eubiosis to post-BMT dysbiosis. Because GVHD is associated with post-transplant dysbiosis, we examined whether prevention of post-transplant dysbiosis would mitigate GI GVHD (Figure 3A). B6 animals received allogeneic BMT (described in STAR Methods). Each individual recipient mouse was cohoused with an individual naive B6 WT mouse in a single cage from day 14 after HSCT. Simpson diversity and principal component analysis (PCoA) of stools from these recipient mice revealed that cohoused allogeneic mice (Allo B6 cohoused with B6 for 2 weeks) had higher diversity and different microbiota compositions from single housed allogeneic mice (Allo B6 not cohoused) (Figures 3B–3F) demonstrating that the cohousing shifted the stool microbiome of Allo B6 recipients toward the healthy microbiome. Cohoused Allo B6 recipients demonstrated greater survival, reduced weight loss, and milder clinical GVHD than not cohoused Allo B6 (Figures 3G–3I). Taken together, the data demonstrate that dysbiosis pre-transplant per se are not disease enhancing, but that promoting post-BMT eubiosis ameliorates the severity of GVHD.

The above effects could be secondary to pre-existing microbiota or from the experimental effects of gavage and antibiotic use. Therefore, to determine whether dysbiotic stool has any intrinsic pathogenic effects and eubiosis has beneficial effects in the absence of above variables, we next compared weight gain of GF mice with littermate GF mice that were conventionalized with either dysbiotic allo-stool or eubiotic syngeneic stool (Figure 4A). GF animals that received eubiotic stool from syngeneic mice and those that were conventionalized with dysbiotic allo-stools demonstrated weight gain when compared with GF controls confirming that dysbiotic microbiome by itself is not pathogenic in the absence of prior damage (Figures 4A–4C and S4A).

Absence of host microbiome aggravates GVHD

Our data demonstrate that changes in endogenous GI microbiome structure after allo-HCT are not a cause but a consequence of GVHD and suggest that they might play a salutary role after BMT.[3,4,16,22,23] However, before the advent of stringent GF facilities, and before technologies to confirm presence of microbes such as 16S sequencing, GF mice exhibited reduced GVHD,[10] suggesting an overall pathogenic role for host microbiome. Therefore, to elucidate the importance of microbiota definitively, and directly, in the gut before BMT, we next hypothesized that in contrast to the current paradigm, GF recipients will demonstrate greater GVHD than normal specific pathogen-free (SPF) animals. To rule out any potential confounding littermate effects at birth between GF and SPF conditions, age-matched GF B6 littermate mice were first separated into two cohorts at 4–6 weeks of age. One group was continued under stringent GF conditions and the second group was aged under SPF conditions up to age 12–14 weeks. These GF and SPF cohorts were then irradiated and transplanted with either syngeneic B6 or allogeneic BALB/c donors and were followed post-BMT under stringent GF or SPF conditions, respectively. All the syngeneic recipients from both the GF and SPF cohorts survived and showed no signs of GVHD, demonstrating that absence of microbiome did not cause mortality in the absence of allo-reactive T cell-mediated damage. All allogeneic recipients under SPF

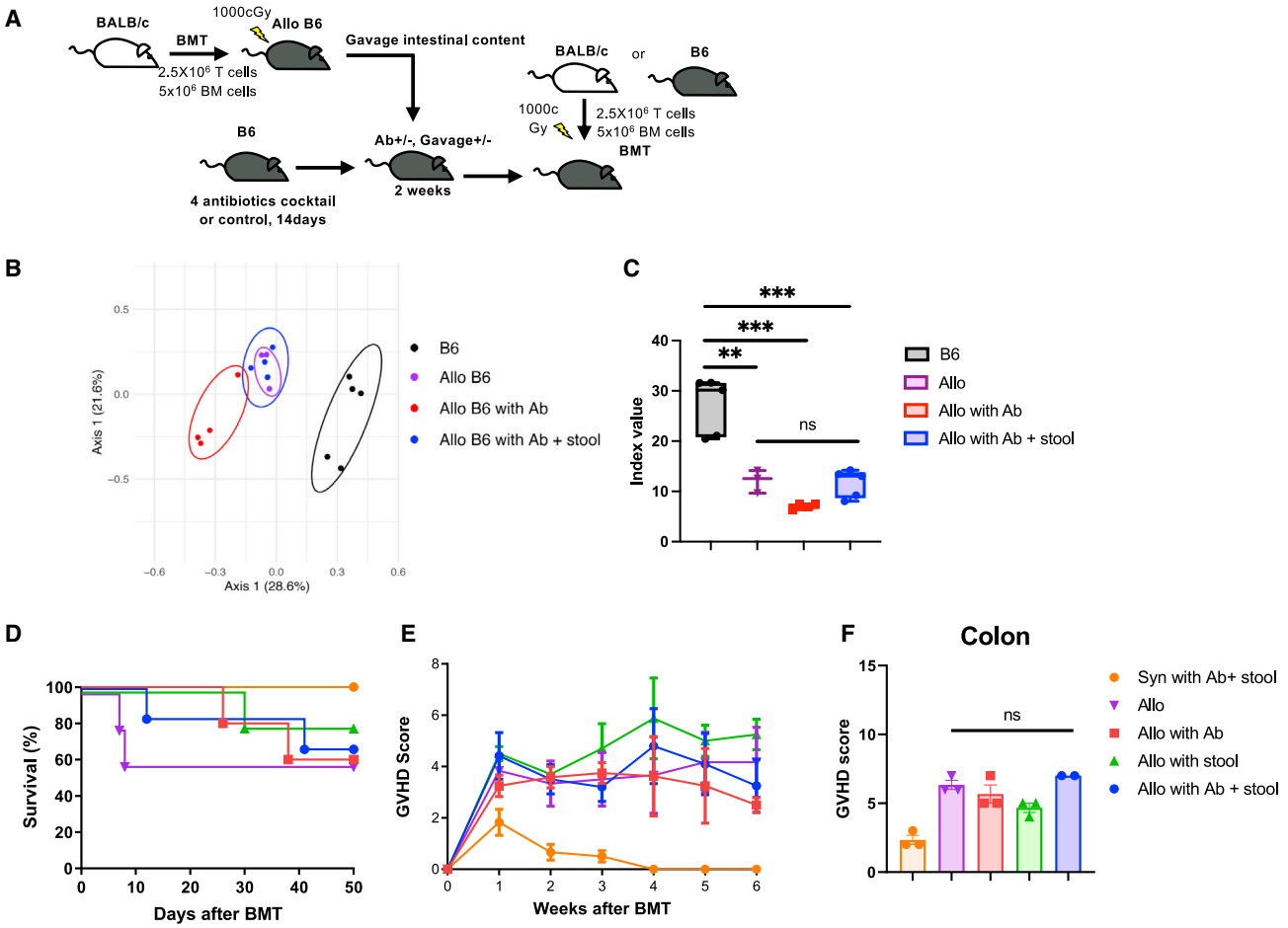

Figure 2. Pre-transplant dysbiosis or eubiosis does not have significant impact on GVHD

(A) B6 mice were treated for 2 weeks with 4 antibiotics cocktail (Figure 1G) or PBS, followed by gavaged Allo B6 intestinal content or PBS. After antibiotics treatment and intestinal content gavage, mice received BMT.

(B and C) Stool from BMT recipients and B6 mice was analyzed by 16S rRNA gene sequencing. PCoA (B) and inverse Simpson alpha diversity index of microbiome (C) are shown. (B6 N = 5, allo N = 3, allo with Ab N = 4, allo with Ab + stool N = 4.)

(D–F) Survival rate (D), clinical GVHD score (E), and pathological GVHD score of colon (F) are shown. (D) Allo: N = 3, allo with Ab: N = 4, allo with Ab + stool: N = 4, B6: N = 5. (E) Syn with Ab + stool: N = 6, allo: N = 5, allo with Ab: N = 5, allo with stool: N = 5, allo with Ab + stool: N = 6. (F) Syn with Ab + stool: N = 3, allo: N = 3, allo with Ab: N = 3, allo with stool: N = 3, allo with Ab + stool: N = 2.

Two independent experiments were performed. One-way ANOVA analysis with Tukey post hoc test (C) and one-way ANOVA analysis with Dunn's post hoc test (F) were used to determine significance (mean ± SEM). $^{**}p < 0.01$, $^{***}p < 0.001$.

See also Figure S3.

conditions, as expected, demonstrated signs of GVHD with a median survival of 7 weeks (Figures 4D–4F). However, the GF mice that received allogeneic HSCT demonstrated greater mortality, weight loss, and clinical GVHD (Figures 4D–4F).

Because allo-stool (dysbiotic microbiome) neither caused disease nor improved weight gain in GF mice, while eubiotic microbiome improved weight gain in GF animals, we next surmised that GF mice transplanted with healthy microbiome will show reduced GVHD. To this end, GF animals received allo-stool or syngeneic stool (Figure 4G). The engraftment and fidelity of the transplanted microbiome was confirmed (Figures S4B–S4D). These animals were then irradiated and utilized as recipients of either syngeneic or allogeneic BMT as in STAR Methods (Figure 4G). Syngeneic recipients that received dysbiotic microbiome survived, demonstrating, once again, no inherent toxicity from the dysbiotic stool. The allogeneic recipients of dysbiotic stool demonstrated expected GVHD mortality and clinical/pathological GVHD (Figures 4H–4J). By contrast, allo-recipients that were transplanted with eubiotic healthy microbiome demonstrated greater survival and reduced weight loss and clinical/pathological GVHD (Figures 4H–4J). Thus, the structure of the host microbiome is dispensable for induction of GVHD but is critical for regulation of GVHD after it has been initiated.

Loss of intestinal physiologic hypoxia causes dysbiosis

We next explored the mechanisms for development of dysbiosis following allo-BMT. The physiologic hypoxia (low oxygen) present at homeostasis in the intestinal milieu regulates the composition and structure of the intestinal microbiome.[1] In the context allo-BMT, host IECs demonstrate a metabolic defect in OXPHOS

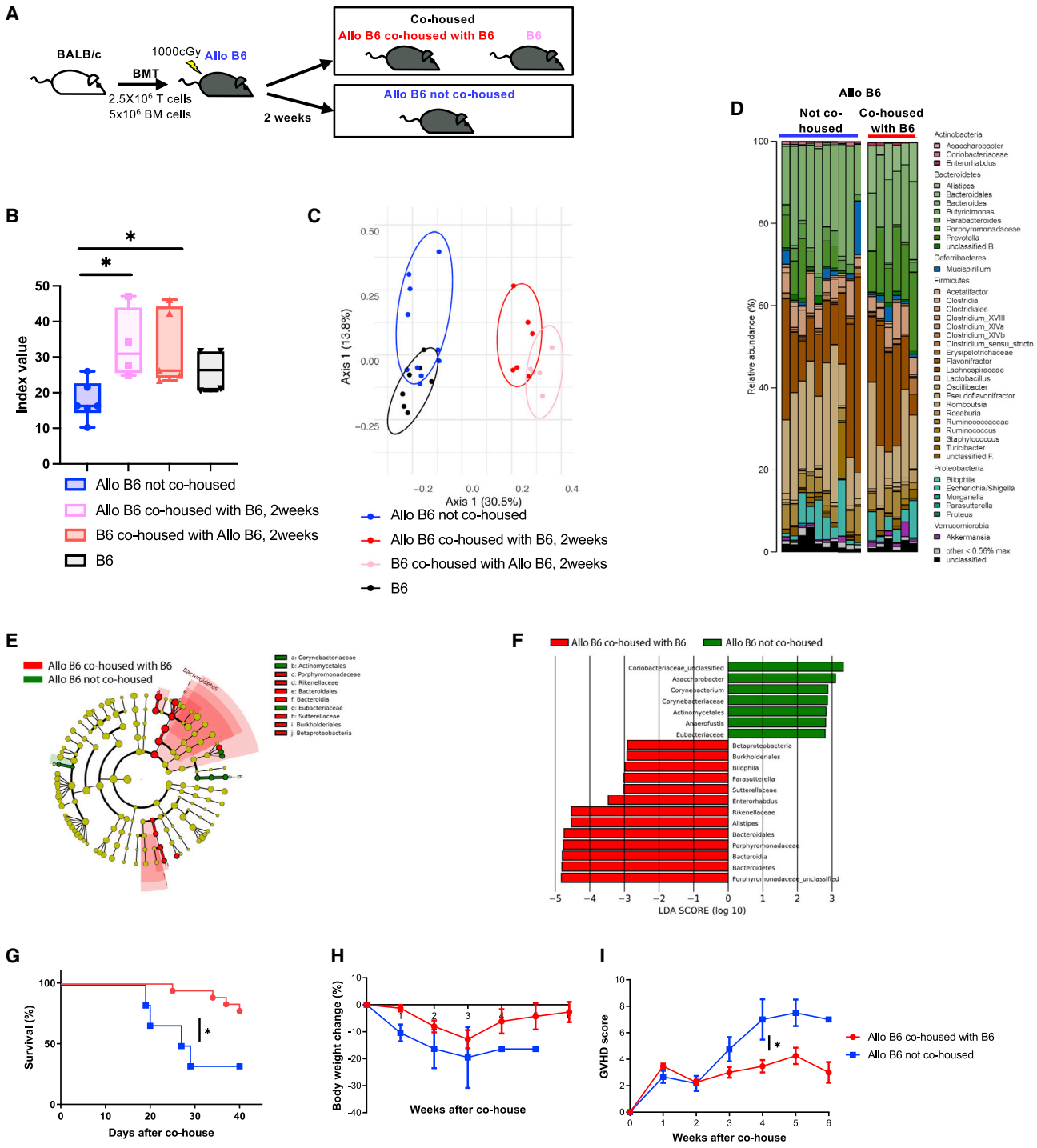

Figure 3. Post-transplant eubiosis ameliorates the severity of GVHD

(A) Allo B6 were cohoused with B6 at ratio of Allo B6: B6 = 1:1 from day 14 after BMT. Data are from three independent experiments.

(B–F) Stool from Allo B6 cohoused with B6 for 2 weeks, B6 cohoused with Allo B6 for 2 weeks, Allo B6 not cohoused, and B6 was analyzed by 16S rRNA gene sequencing.

(B) Inverse Simpson alpha diversity index were shown. (Allo B6 not cohoused: N = 6, Allo B6 cohoused with B6: N = 4, B6 cohoused with Allo B6: N = 5, B6: N = 4.)

(C) PCoA were shown (Allo B6 not cohoused: N = 9, Allo B6 cohoused with B6: N = 6, B6 cohoused with Allo B6: N = 5, B6: N = 7).

(D–F) Microbiome composition (D) and taxa differentially abundant by LEfSe analysis (E and F) are shown.

(legend continued on next page)

due to a T cell-induced disruption of mitochondrial complex II.[21] We therefore hypothesized that lack of utilization of cellular O_2 caused by disruption of OXPHOS in the IECs after allo-HCT will lead to loss of physiologic hypoxia (increase in O_2) and thus cause dysbiosis by making the GI tract more permissive for growth of aerotolerant and facultative anaerobes at the expense of obligate anaerobes. To this end, we systematically measured oxygen consumption of IECs, the changes in the intestinal luminal and mucosal levels of O_2 by colonoscopy, and intestinal cellular hypoxia by pimonidazole after HSCT. B6 received either syngeneic B6 or allogeneic BALB/c transplants as in STAR Methods. Consistent with previous reports, $CD326^+$ IECs harvested from the allogeneic mice on day 21 after HSCT demonstrated a reduction in oxygen consumption rate (OCR) when compared with IECs from syngeneic controls (Figure 5A). Furthermore, IECs from allogeneic animals did not respond to treatment with carbonyl cyanide-p-trifluoromethoxyphenylhydrazone (FCCP), a mitochondrial uncoupler, when compared with IECs from syngeneic animals demonstrating the reduction in allo-IEC mitochondrial electron transport chain (ETC) functions and utilization of O_2 (Figure 5A). However, both syngeneic and allogeneic IECs showed similar extracellular acidification rates (ECARs, an indicator of glycolysis), with reduced OCR/ECAR ratio (Figure S5A). This suggests that the defect in O_2 utilization should increase O_2 levels, leading to a loss of intestinal luminal and cellular physiological hypoxia.

To confirm the increased O_2, we performed colonoscopy with probes that directly measure oxygen levels in the colonic mucosa (adjacent to IECs) and in the center the intestinal lumen of the HSCT recipients. The O_2 concentrations in deeper locations, in the inner mucus of the colon, immediately adjacent and closer to the IECs was greater in the allo-recipients than the controls (Figure 5B). The oxygen levels in the lumen, further away from the IECs initially demonstrated similar levels of oxygen in allo-recipients as in the controls naive or syngeneic B6 controls early after BMT (Figure 5B). However, 3 weeks after BMT, the allo-recipients demonstrated greater levels of O_2 in the intestinal lumen when compared with the controls demonstrating a loss of hypoxia in the lumen farther away from the IECs (Figure 5B). Finally, loss of intestinal cellular hypoxia with pimonidazole was also documented in the allo-BMT recipients at days 7 and 21 after HSCT (Figure 5C). Thus, underutilization of the O_2 by the IECs because of T cell-induced metabolic defect leads to loss of intestinal physiological hypoxia in GVHD.

Next, to validate whether the loss of physiological intestinal hypoxia is exclusively from T cell-mediated GVHD and not a consequence of strain-dependent artifacts or damage from conditioning, we determined the status of intestinal hypoxia in the non-irradiated parent into F1 model (B6 → B6D2F1), where alloreactive donor T cells cause GVHD despite absence of conditioning (Figures S5B and S5C). Allogeneic IECs demonstrated increased levels of oxygen (Figure 5D). Similar loss of hypoxia was also observed when allogeneic B6 animals were conditioned with chemotherapy (busulfan and cyclophosphamide) prior to HSCT (Figure 5E). By contrast, when animals were conditioned with irradiation alone hypoxia was maintained (Figure 5F). To demonstrate that the loss of physiological hypoxia is independent of microbiome composition, we utilized mouse strains from a different mouse supplier (Taconic, JAX). Allogeneic Taconic B6, Taconic BALB/c, and JAX BDF1 recipients showed similar loss of hypoxia at day 7 after BMT (Figures S5D–S5F). These results extend previous observations and demonstrate that the increase in O_2 concentration in the intestines is observed only in the context of allo-T cell-mediated damage of GI tract.[21] To further determine whether this can be extended to other T cell-mediated GI damage, we determined intestinal oxygen concentration in the $CD45RB^{hi}$ adoptive T cell-mediated autoimmune model of IBD. Induction of T cell-mediated autoimmune colitis also led to loss of hypoxia in both SPF (Figures 5G and S5G) and GF animals (Figures 5H and S5H). Thus, T cell-mediated disruption of intestinal cell OXPHOS in the IECs leads to poor utilization of cellular O_2 resulting in loss of physiologic hypoxia that promotes an environment permissive for dysbiosis.

Next, to enhance the generalizability and demonstrate that loss of physiological hypoxia is not an artifact of the specific vivarium conditions, we performed the similar experiments with different strain combinations at a second institution (MSKCC, NY Center). Similar to the data from University of Michigan, HCT recipients with GVHD showed loss of hypoxia in colon (Figure 6A). Changes in microbiome composition (Figure 6B) and decreased ratio of obligate/facultative anaerobes in recipients with GVHD (Figure 6C) were observed. These data demonstrated GVHD induced loss of hypoxia and dysbiosis in colon is independent of the institution, vendors, and strains.

Intestinal O_2 levels regulate GVHD in a microbiome-dependent and -independent manner

We determined whether the loss of physiologic hypoxia has a direct effect on IECs that could impact GI GVHD. To analyze the impact of increase in O_2, we determined the expression of cellular O_2 sensor, HIF-1α. B6 animals received syngeneic or allogeneic BMT (see STAR Methods). *Hif-1*α gene expression was similar in the IECs harvested from allogeneic and syngeneic animals (Figure 6A). However, the HIF-1α protein was reduced in the IECs from allogeneic animals when compared with syngeneic animals on day 21 after BMT (Figure 7B). By contrast, the expression of proryl hydroxylase 3 (PHD3), a protease that regulate the protein level of HIF-1α, was increased in the allo-IECs (Figures 7C and 7D)

Next, to determine whether the IEC cell-autonomous loss of physiologic hypoxia after allo-HSCT has a microbiome-independent effect on GI GVHD, we utilized littermate congenic IEC-specific Hif-1*a* gene knockout mice (*Hif1a*$^{fl/fl}$ *Villin1*^{cre} B6) or the WT *Hif1a*$^{fl/fl}$ B6 animals (to harmonize pre-HCT microbiome) as allogeneic HSCT recipients. The animals were cohoused post-BMT to harmonize microbiome changes. The IEC-specific *Hif1a*$^{fl/fl}$

(G–I) Survival rate (G), body weight change (H), and clinical GVHD score (I) of BMT recipients were shown. (Allo B6 were cohoused with B6: N = 18, Allo B6 not cohoused: N = 6.)

The horizontal line in box (B) represents the median with the box bounding the interquartile range. The ends of the whisker lines represent the minimum and maximum values. One-way ANOVA analysis with Tukey post hoc test (B), log-rank test (G), and two-tailed Mann-Whitney test (I) were used to determine (mean ± SEM). *$p < 0.05$.

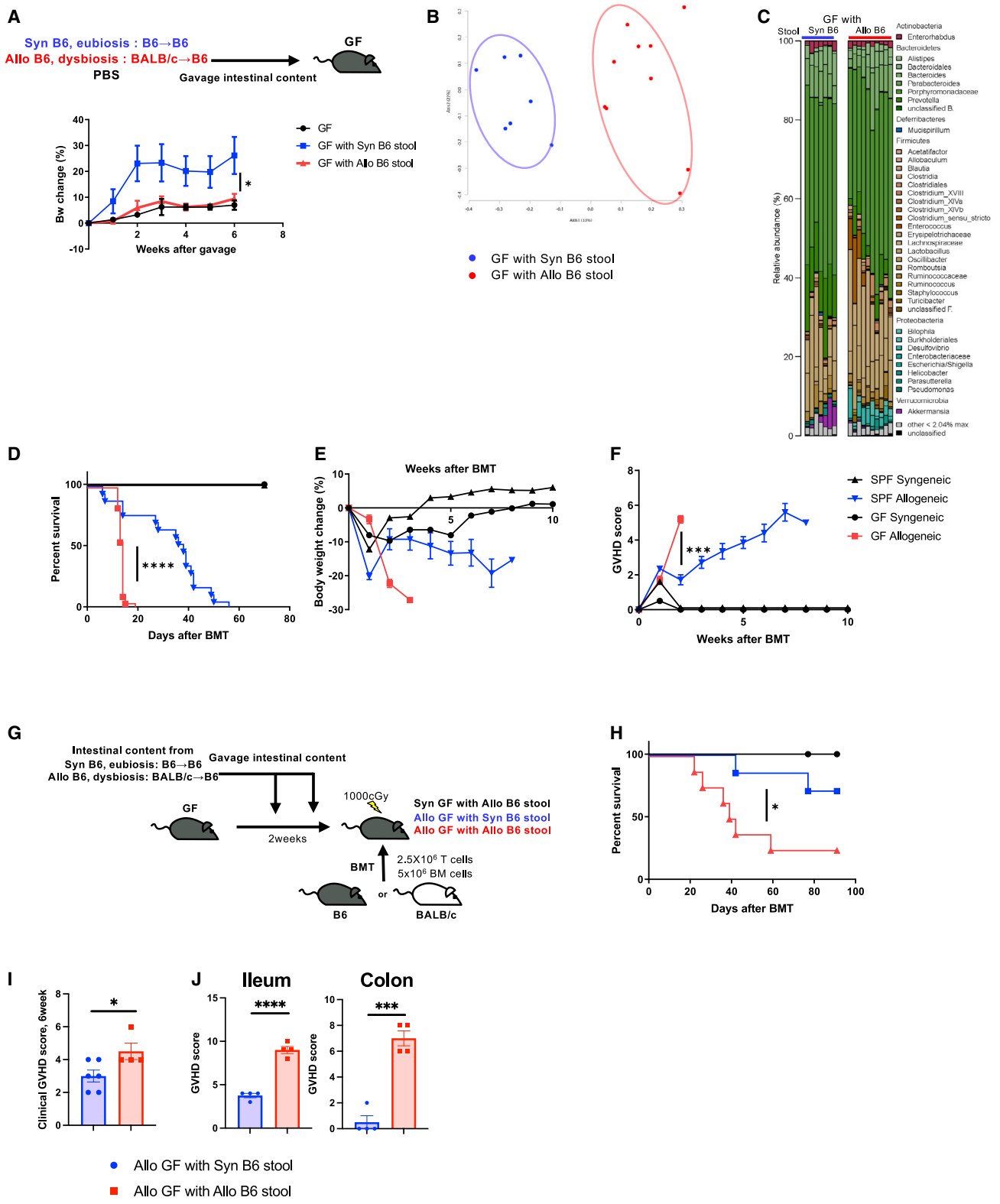

Figure 4. GF mice transplanted with healthy microbiome showed reduced GVHD

(A–C) Germ-free B6 (GF) mice were gavaged intestinal content from Syn and Allo-BMT-recipient mice.

(A) Body weight change is shown (GF: N = 2, GF with Syn B6 stool: N = 4, GF with Allo B6 stool: N = 5). Stool from GF with Syn or Allo B6 stool 4 weeks after stool gavage analyzed by 16S rRNA gene sequencing.

(legend continued on next page)

Villin1^{cre} B6 allogeneic recipients showed greater GVHD severity and mortality, compared with the littermate *Hif1a*$^{fl/fl}$ B6 mice despite being cohoused (Figures 7E and 7F). Taken together, these data demonstrate that changes in O_2 after allo-HSCT directly affect host IECs, enhancing GVHD severity independent of changes in the microbiome.

We next determined the direct functional link between the increase in O_2, the loss of physiologic hypoxia, observed after allo-HSCT to the resultant dysbiosis and GVHD severity. To mitigate the impact of excess luminal O_2 by reducing the Fenton reaction in the IECs, we administered the iron chelator, deferasirox, by oral gavage after BMT (see STAR Methods).[24,25] We determined the experimental dose and timing by measuring the level of iron in the stool from both small and large intestines following gavage with Fe chelator (Figure S6A). We first determined whether gavaging with deferasirox altered the level of O_2 concentration in the intestines after HSCT and found that it mitigated loss of hypoxia in the allogeneic recipients (Figure 7G). The PCoA analysis showed different microbial composition between vehicle and deferasirox-treated allogeneic animals (Figure 7H), with an increase in microbial diversity (Figures 7I and 7J) thus demonstrating that changes in O_2 directly contributed to dysbiosis after allo-HSCT. We next hypothesized that squelching of O_2 to ameliorate dysbiosis after allo-HSCT will lead to attenuation of GVHD mortality. Consistent with the hypothesis, deferasirox-treated allogeneic animals demonstrated reduced severity of clinical GVHD and survival (Figures 7K and 7L). The iron chelator did not show any effect on inflammatory cytokine secretion and Treg ratio in spleen (Figures S6B and S6C).

Because alteration of O_2 affects both host IECs and the microbiome, we next determined whether restoring intestinal hypoxia by Fe chelation after allo-HSCT mitigated GVHD independent of its impact on dysbiosis. To determine microbiome-independent effects, we utilized GF B6 animals as allo-HSCT recipients and treated them with deferasirox or diluent control (see STAR Methods). All transplanted mice were maintained in stringent GF environment post-BMT. Treatment with Fe chelation ameliorated loss of hypoxia after BMT in the GF recipients (Figure S6D). All syngeneic GF mice treated with either diluent control or deferasirox survived without GVHD. The allogeneic GF mice treated with diluent control demonstrated severe GVHD and died within 2 weeks after BMT (Figures S6E and S6F). By contrast, deferasirox-treated allogeneic GF mice (Figures S6E and S6F) demonstrated improved survival when compared with diluent treated allo-recipients but eventually succumbed to GVHD. These data collectively demonstrate that O_2 modulation, to improve intestinal physiologic hypoxia, has direct salutary effects both on host IECs and the host microbiome to improve GI GVHD.

DISCUSSION

Colonic dysbiosis is associated with human intestinal diseases, including GI GVHD and IBD.[1,9] However, whether dysbiosis is a cause or consequence, an amplifier or a mollifier, and the mechanisms remain elusive. Herein, we address these gaps and demonstrate that pre-transplant dysbiosis by itself is not pathogenic, but rather post-HCT dysbiosis is a consequence of the changes in intestinal luminal oxygen level from the tissue injury caused by allogeneic donor T cells after allo-HCT. We additionally demonstrate that correction of post-transplant dysbiosis has beneficial impact. We show that in contrast to the existing paradigm, absence of microbiome after HCT aggravates GVHD, and thus provide clarity to the emerging data that the structure of the microbiome after HCT, regulates the severity of GI GVHD.[3,10,16,17,21,22] These data extend previous observations that T cell-mediated disruption of intestinal OXPHOS leads to the loss of luminal physiological hypoxia (increase in O_2),[21] which functions as a control switch to shift the intestinal microbiome from predominantly obligate anaerobes to facultative anaerobes and aerotolerant microbes, thus providing mechanistic insights into the cause of dysbiosis. Finally, targeting excess O_2 with iron chelation promoted physiologic hypoxia, mitigated dysbiosis, and attenuated GVHD severity, thus suggesting that Fe chelation with available oral drugs may be a novel strategy to clinically mitigate GVHD severity.

During homeostasis, the host IEC metabolism is dependent on OXPHOS resulting in high epithelial oxygen consumption and as a consequence epithelial and luminal hypoxia.[1] Epithelial hypoxia helps to maintain a microbial community dominated by obligate anaerobic bacteria at homeostasis.[1,20] We build on prior observation that the disruption of host IEC metabolism pathogenic T effector cells results in an increase in intestinal oxygen, thereby driving an expansion of facultative anaerobic and aerotolerant bacteria, a hallmark of dysbiosis GVHD.[4,22,23] Thus, one critical mechanism for dysbiosis, the loss of physiologic hypoxia in a non-infectious intestinal diseases such as GVHD and IBD are similar to that observed following infection by enteric infectious pathogens.[1,22] This shared mechanism linked to tissue oxygenation in causing dysbiosis allows for a better understanding of other diseases associated with dysbiosis. It is however possible that the dominant mechanisms of dysbiosis may be distinct in different systemic diseases.

Seminal studies suggested that GF hosts had less severe GVHD.[9,10] These studies formed a paradigm for the field of HCT, even as they appeared to stand in contrast to emerging data implicating strong correlation between microbiome and GVHD. The modern-day studies, however, showing shifts in

(B and C) PCoA (B) and microbiome composition (C) are shown (GF with Syn B6 stool: N = 7, GF with Allo B6 stool: N = 10).
(D–F) SPF B6 and GF B6 mice received BMT from B6 or BALB/c donor. Survival rate (D), body weight change (E), and clinical GVHD score (F) are shown (GF syngeneic: N = 2, GF allogeneic: N = 18, SPF syngeneic: N = 2, SPF allogeneic: N = 17).
(G–J) GF B6 mice received BMT from B6 or BALB/c donor. Then GF mice were gavaged intestinal content from SPF Syn and SPF Allo-BMT-recipient mice (G). Survival rate (H) and clinical GVHD score 6 weeks after BMT (I) are shown (allo GF with Syn B6 stool N = 6, allo GF with Allo B6 stool N = 4). (J) Ileum and colonic histopathological score at day 7 after BMT are shown (n = 4).
Two-tailed unpaired t test (A, I, and J), log-rank test (D and H), and two-tailed Mann-Whitney test (F) were used to determine (mean ± SEM). *$p < 0.05$, ***$p < 0.001$, ****$p < 0.0001$.
See also Figure S4.

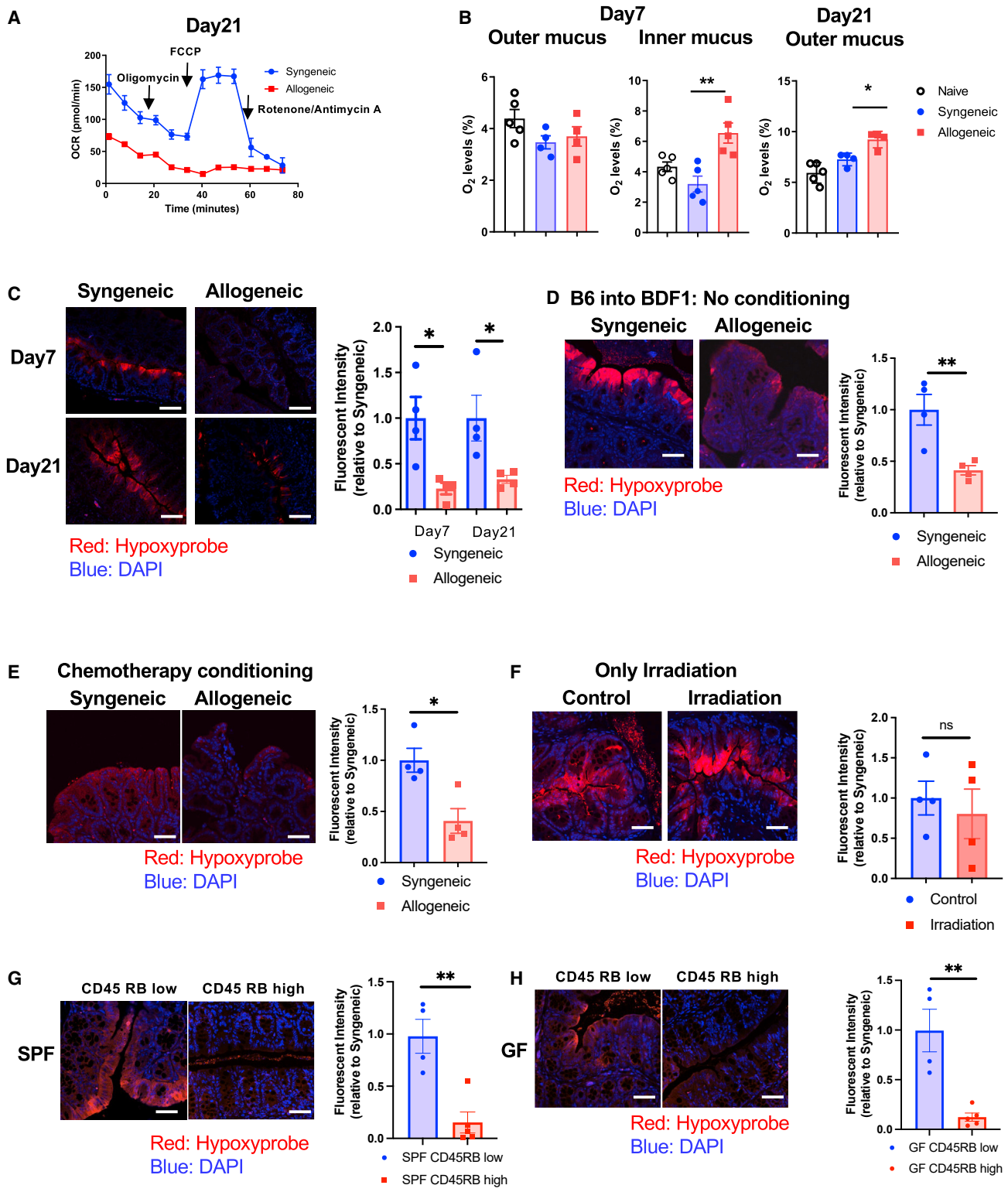

Figure 5. The defect in O_2 utilization in IECs leading to a loss of intestinal luminal and cellular physiological hypoxia

(A) Representative bio-energetic profiles of isolated colonic IECs from syngeneic and allogeneic mice (BALB/c → B6) under basal conditions and following treatment with mitochondrial inhibitors (oligomycin, FCCP, rotenone/antimycin A) by Seahorse analyzer. Oxygen consumption rate (OCR) of day 21 after BMT is shown (N = 4). Four independent experiments were performed.

(B) Quantification of O_2 levels in intestine from recipients 7 and 21 days after BMT (BALB/c → B6). Naive: N = 5, syngeneic: N = 4 (day 7 outer and day 21 outer), N = 5 (day 7 inner), allogeneic: N = 4 (day 7 outer and day 21 outer), N = 5 (day 7 inner).

(legend continued on next page)

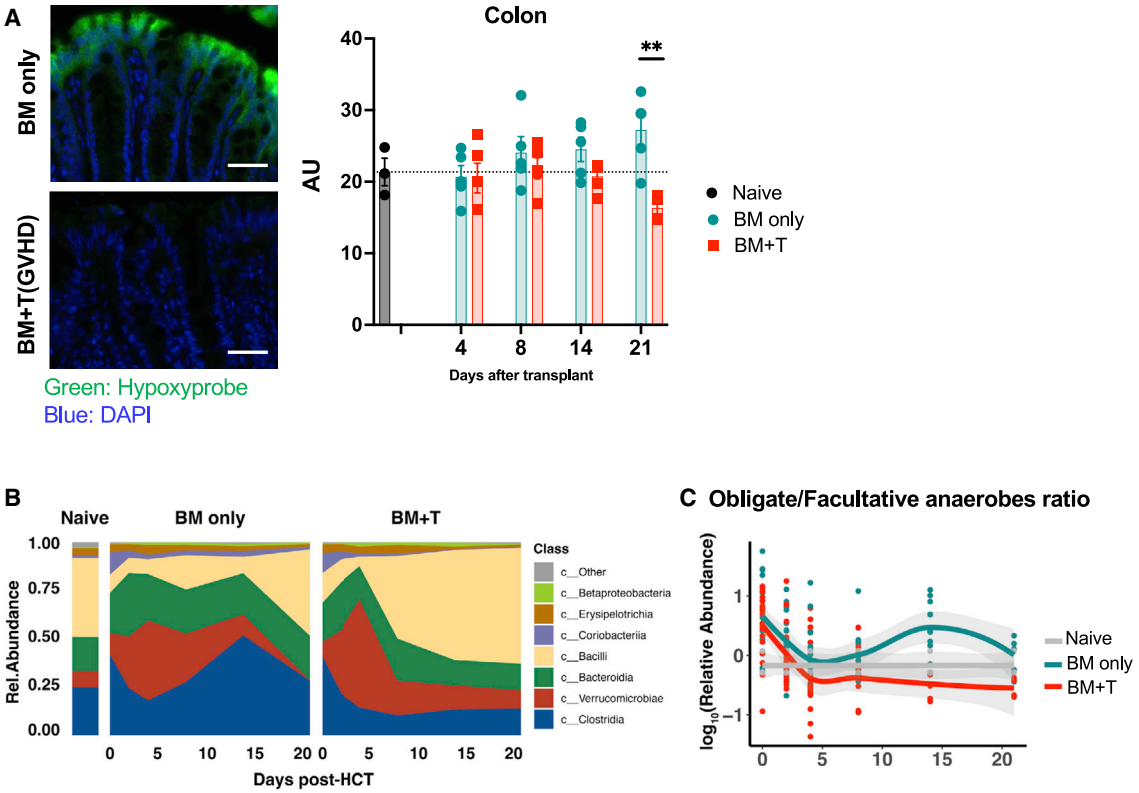

Figure 6. Loss of hypoxia in colon and dysbiosis are induced by GVHD with independent of the different institution and microbiome

Lethally irradiated (1,000 cGy) 129 mice received bone marrow (5 × 10^6 cells) and purified $CD5^+$T cells (2 × 10^6 cells) from C57BL/6J donors in different institution (Memorial Sloan Kettering Cancer Center).

(A) Tissue hypoxia was determined with pimonidazole (left, scale bars, 50 μm). Quantification of intestinal O_2 levels in intestine from recipients (right). Samples were collected 4, 8, 14, and 21 days after BMT (naive: N = 3, BM only: N = 4, BM + T: days 4, 8, and 14 N = 4, day 21 N = 3).

(B) Stool microbial composition was determined by 16S rRNA gene sequencing.

(C) The classification of obligate/facultative (O/F) anaerobe ratio was determined.

Two-tailed unpaired t test (A) was used to determine significance (mean ± SEM). **p < 0.01.

microbiome or use of antibiotics as potential regulators of GVHD, do not address the notion of stringent GF status on GVHD. We evaluated the role of stringent GF status on GVHD and found that complete absence of microbiome in transplanted mice that are housed in GF conditions show greater severity and mortality from GVHD than normal SPF recipients. These data directly demonstrate an overall salutary role for microbiome in GVHD. The reason for the different results from the studies by van Bekkum et al. is likely because those earlier studies were performed in an era when sequencing for microbiome was not yet available and as such the ability to confirm true GF status or the reliability of the colony conditions to be maintained in a GF state was likely not optimal.[10,26] Furthermore, our data demonstrate that adding back enteric microbiome mitigated GVHD severity in GF hosts, thus definitively demonstrating a critical role for microbiome in regulation of GVHD.

(C) B6 received BMT from B6 or BALB/c donor. Representative images of hypoxyprobe staining and relative fluorescent intensity in colon from recipients 21 days after BMT (scale bars, 50 μm).

(D) Unirradiated B6D2F1 mice received 10 × 10^7 splenocytes from syngeneic B6D2F1 or allogeneic B6 donors. Representative images of hypoxyprobe staining and relative fluorescent intensity in colon from recipients at 21 days after BMT (scale bars, 50 μm) (N = 4).

(E) B6 mice received chemotherapy and received 1 × 10^7 T cells along with 1 × 10^7 TCD-BM cells from either syngeneic B6 or allogeneic BALB/c donors. Representative images of hypoxyprobe staining and relative fluorescent intensity in colon from recipients 21 days after BMT (scale bars, 50 μm) (N = 4).

(F) B6 mice received 10 Gy total body irradiation without T cell and BM cells. Representative images of hypoxyprobe staining relative fluorescent intensity in colon from recipients 7 days after BMT (scale bars, 50 μm) (N = 4).

(G and H) CD4++CD25−CD4+4-CD4+5RBhi (CD4+5RB high) T cells or CD4++CD25−CD4+4-CD4+5RBlow (CD4+5RB low) T cells from B6 mice were transferred to Rag1−/− SPF (G) or Rag1−/− GF mice (H). Hypoxyprobe staining and relative fluorescent intensity in colon from recipients 8 weeks after T cell transferring (scale bars, 50 μm) (SPF: N = 4, GF CD4+5RB low: N = 4, GF CD4+5RB high N = 5).

(C–H) At least four independent experiments were performed. One-way ANOVA analysis with Tukey post hoc test (B) and two-tailed unpaired t test (C–H) were used to determine significance (mean ± SEM). *p < 0.05, **p < 0.01.

See also Figure S5.

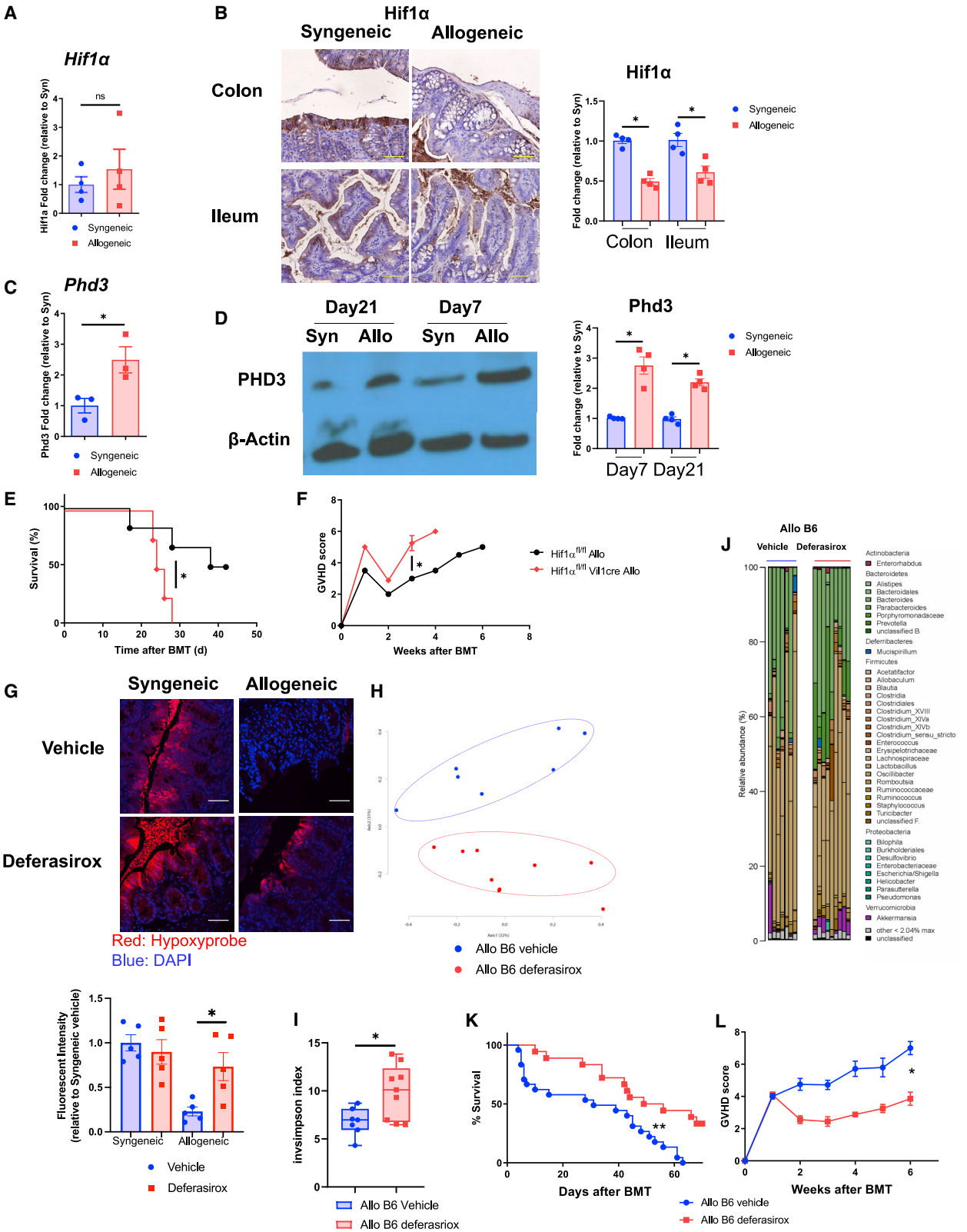

Figure 7. O_2 modulation after allo-HSCT improves intestinal physiologic hypoxia and GVHD

(A–D) B6 received BMT from syngeneic B6 or allogeneic BALB/c donor.

(A) Hif1α mRNA expression of isolated colonic IECs from BMT recipients 21 days after BMT (N = 4).

(legend continued on next page)

Our data utilizing cohousing SPF, antibiotic-treated, and GF animals provide several insights into the role of dysbiosis before and after allo-HCT. First, dysbiosis by itself, in the absence of initial damage by alloreactive T cells, is not pathogenic, at least in the period that acute GVHD mortality typically occurs in these systems. Second, the presence of dysbiosis prior to HCT did not aggravate GVHD. However, promotion of eubiosis after HCT mitigated GVHD. Similarly, GF mice conventionalized with healthy stools mitigated GVHD. These data, when taken together with observations that outcomes are worse in humans with use of antibiotics that primarily target anaerobes after HCT demonstrate that microbiome primarily has a salutary role in GVHD. Thus, promotion of eubiosis after HCT (i.e., prebiotic or probiotic approaches with appropriate antibiotic stewardship for growth of healthy microbiome, i.e., obligate anaerobe microbes) as opposed to treating dysbiosis before (eliminating facultative anaerobes or aerobes, i.e., only antibiotic approaches) may be a rational strategy to therapeutically modulate microbiome to ameliorate GVHD. The mechanisms by which eubiosis after HCT may mitigate GVHD is likely (but not limited) to generation of metabolites by obligate aerobeic commensals that nourish the IECs, or promote immune and tissue tolerance, or provide nutrients to healthy commensals and regulate the microbial ecology by promoting a milieu that is not permissive for pathobionts.[16,17,21,27–30] However, the biology of GVHD is complex with several studies demonstrating a role for damage-associated molecular patterns (DAMPs) and pathogen-associated molecular pattern (PAMP) production by tissue damage as amplifiers of a GVH response.[31,32] Therefore it is possible that dysbiosis when characterized by expansion of pathobionts that gain access to hosts circulation and tissues amplifies GVHD.[4,22,33]

The increase in, and the type of pre-transplant dysbiosis noted in the clinical studies that correlated with outcomes suggest that factors that lead to dysbiosis could predict worse GVHD, but do not directly demonstrate that dysbiosis by itself directly caused GVHD. Nonetheless, it is possible, even if unlikely based on our GF reconstitution experiments, that there might be a threshold for the specific type, or degree of dysbiosis, beyond which pre-transplant dysbiosis may cause or promote GVHD. The change in specific bacteria (*Enterococcus* and reduction in *Blautia*) has been hard to compare between different studies, but nonetheless, all of the studies are broadly consistent with reduction in obligate anaerobes and an increase in proportion of aerotolerant microbiome following GVHD. Thus, the nature of specific microbes and their impact in the context of the wider ecology will need to be assessed in future studies with GF mice monocolonized or polycolonized with depletion of specific microbe of interest to directly assess their pathogenic or beneficial effects, alone, and in the context of other microbes. However, our observations, regarding the hypoxia loss in GVHD and the development of dysbiosis, are consistent across vendor source, different strains, multiple model systems, and under different experimental conditions from different institutions.

It remains unknown whether the degree of GVHD severity affects microbiome contents in a specific manner. However, our data, consistent with previous data, have shown that there is a general loss of diversity. It remains to be determined whether the measurement such as the specific and absolute loss of diversity can be consistently quantified and compared across different patients and contexts, and to formally assess and rule out that the degree of dysbiosis may directly cause GVHD. Additionally, the improvement of survival in cohousing experiments could be confounded by the social, behavioral, or neurological effects of cohabitation, besides, or in addition to, changes in microbiome. These potential variables will need to be investigated in carefully designed future studies.

During homeostasis, despite being in a relative hypoxic environment, intestinal metabolism is directed toward OXPHOS, resulting in high epithelial oxygen consumption. Disruption of OXPHOS in the IECs by alloreactive T cells, reduces oxygen consumption.[21] Our data now extend these observations and provides a potential novel therapeutic approach. It demonstrates that increase in luminal oxygen makes the intestinal environment less permissive for obligate anaerobes, thus promoting dysbiosis. The excess tissue oxygen levels is also corroborated by lower expression of the O_2 sensor HIF-1α in the IECs.[34–36] It is likely that the lack of O_2 consumption might also contribute by direct free radical injury to the IECs and increase GVHD severity. Administration of oral iron chelator reduced excess luminal O_2, promoted physiological hypoxia, improved microbial diversity, reduced dysbiosis, and ameliorated GI GVHD but did not alter donor T cell immune responses in the host. Moreover, oral Fe chelation also modestly improved GVHD survival in GF animals demonstrating microbiome-independent effects. Thus, squelching of excess O_2 by Fe chelation improved GI GVHD largely in a microbiome-dependent, but also, to a modest degree, in a microbiome-independent manner. The specific mechanisms for microbiome-independent effects of Fe chelation on host tissues, such as ferroptosis, will need further investigation.[37,38]

(B) Representative image and the relative intensity of HIF1α immunohistochemical staining with intestinal tissue from BMT recipients 21 days after BMT are shown (scale bars, 50 μm, N = 4).
(C) Egln3 (Phd3) mRNA expression of isolated colonic IECs from BMT recipients on day 21 after BMT (N = 3).
(D) Representative image of immunoblot and the relative protein density for PHD3 and β-actin with colonic IECs from BMT recipients 21 days after BMT are shown (N = 4).
(E and F) Hif1αfl/fl mice and Hif1αfl/fl Vil1cre mice received BMT from BALB/c donor. Survival rate (E) and clinical GVHD (F) score are shown (Hif1$\alpha^{fl/fl}$ allogeneic: N = 6, Hif1$\alpha^{fl/fl}$ Vil1cre: N = 4).
(G–L) B6 received BMT from BALB/c donor mice. BMT recipients were orally treated with deferasirox (20 mg/kg) and vehicle every day. (G) Hypoxyprobe staining and relative fluorescent intensity in colon from recipients 21 days after BMT (scale bars, 50 μm). Four independent experiments were performed. Stool from BMT recipients were analyzed by 16S rRNA gene sequencing. PCoA (H), inverse Simpson alpha diversity index of microbiome (I), and microbiome composition (J) in stool from recipients 21 days after BMT were shown (Allo B6 vehicle: N = 7, Allo B6 deferasirox: N = 9). Survival rate (K) and clinical GVHD score (L) of BMT recipients (Allo B6 vehicle: N = 24, Allo B6 deferasirox: N = 10).
Representative plots and a graph summarizing the results of at least two independent experiments are shown. Two-tailed unpaired t test (A, C, G, and I), two-tailed Mann-Whitney test (B, D, F, and L), or log-rank test (E and K) (mean ± SEM) were used to determine significance. *$p < 0.05$, **$p < 0.01$.
See also Figure S6.

Furthermore, Fe chelation likely impacts Fe availability to microbes directly affecting the structure of microbiome.[39] Nonetheless, our data thus provide a novel role for tissue O_2 as a mechanism for dysbiosis and Fe chelation as a therapeutic target for amelioration of non-infectious immune-mediated intestinal diseases.

Limitations of the study

The study did not address the impact of alterations of oxygen levels on the changes in specific bacterial genus and species. This will need to be carefully dissected in future studies. The lack of deleterious effects of dysbiosis on the GI tract of the hosts were limited to a relatively short duration (6 weeks). The impact on long-term GI or general health of the host will need to be addressed. The effect of the absence or variations in key host immune cell functions such as cytokines, effector responses that affect the host response to dysbiosis and on GVHD severity was not addressed in this study. Iron chelation likely directly impacts the host microbial ecology, such as alterations in siderophore producers. Our study demonstrates a cause for dysbiosis in murine models, but the direct relevance of intestinal ambient oxygen levels to human GI GVHD will need to be analyzed in prospective human studies.

STAR★METHODS

Detailed methods are provided in the online version of this paper and include the following:

- KEY RESOURCES TABLE
- RESOURCE AVAILABILITY
  - Lead contact
  - Materials availability
  - Data and code availability
- EXPERIMENTAL MODEL AND SUBJECT DETAILS
  - Mice
  - Hematopoietic cell transplantation model
  - Colitis models
- METHOD DETAILS
  - Systemic and histopathological analysis of GVHD
  - DNA extraction, 16S rRNA gene sequencing and data analysis
  - Intestinal epithelial cells and intraepithelial cells isolation
  - Preparation of lymphocytes single cell suspension and flow cytometry
  - Immunoblot analysis
  - Immunohistochemistry staining
  - Seahorse analysis
  - Measurements of oxygen concentration in colonic mucosa
  - RNA isolation and RT-PCR
  - Quantification of iron in intestinal content
- QUANTIFICATION AND STATISTICAL ANALYSIS

SUPPLEMENTAL INFORMATION

Supplemental information can be found online at https://doi.org/10.1016/j.immuni.2023.01.007.

ACKNOWLEDGMENTS

This work was supported by the US National Institutes of Health grants P01HL149633 (P.R. and G.D.), HL152605 (P.R.), CA217156 (P.R.), R01CA148828 (Y.M.S.), R01CA245546 (Y.M.S.), and R01DK095201 (Y.M.S.). This work in Memorial Sloan Kettering Cancer Center was supported by National Cancer Institute award numbers R01-CA228358, R01-CA228308, and P30 CA008748; MSK Cancer Center Support Grant/Core Grant and P01-CA023766; National Heart, Lung, and Blood Institute (NHLBI) award numbers R01-HL123340 and R01-HL147584; and TriInstitutional Stem Cell Initiative (M.R.M.v.d.B.).

We acknowledge use of the Microbiome Core, the Microscopy and Image-analysis Laboratory (MIL) and germ-free facility of the University of Michigan's Biomedical Research Core Facilities for the preparation of samples and images. Support for the MIL core is provided by the University of Michigan Rogel Cancer Center (NIH grant CA46592).

AUTHOR CONTRIBUTIONS

P.R. conceived the study. K.S., H.F., I.H., A.K., M.R.M.v.d.B., and P.R. planned, guided the research, analyzed the data, and wrote the manuscript. K.S., H.F., I.H., M.B.d.S., K.O.-W., E.L., L.L., and Y.S. performed experiments. R.H., A.K., R.R.J., and G.D. analyzed 16S RNA sequences experiment. C.L. performed experiments and histopathological analysis. M.H. and T.M.S. performed oxygen measurements in colonic mucosa. Y.M.S. generated the Hif1αfl/fl vilcre mice. P.R. supervised the project.

DECLARATION OF INTERESTS

The authors declare no competing interests.

INCLUSION AND DIVERSITY

We worked to ensure sex balance in the selection of non-human subjects. One or more of the authors of this paper self-identifies as a gender minority in their field of research. While citing references scientifically relevant for this work, we also actively worked to promote gender balance in our reference list.

Received: June 10, 2022
Revised: November 12, 2022
Accepted: January 10, 2023
Published: February 2, 2023

REFERENCES

1. Litvak, Y., Byndloss, M.X., and Bäumler, A.J. (2018). Colonocyte metabolism shapes the gut microbiota. Science *362*, eaat9076. https://doi.org/10.1126/science.aat9076.
2. Byndloss, M.X., Pernitzsch, S.R., and Bäumler, A.J. (2018). Healthy hosts rule within: ecological forces shaping the gut microbiota. Mucosal Immunol. *11*, 1299–1305. https://doi.org/10.1038/s41385-018-0010-y.
3. Shono, Y., Docampo, M.D., Peled, J.U., Perobelli, S.M., Velardi, E., Tsai, J.J., Slingerland, A.E., Smith, O.M., Young, L.F., Gupta, J., et al. (2016). Increased GVHD-related mortality with broad-spectrum antibiotic use after allogeneic hematopoietic stem cell transplantation in human patients and mice. Sci. Transl. Med. *8*, 339ra71. https://doi.org/10.1126/scitranslmed.aaf2311.
4. Peled, J.U., Gomes, A.L.C., Devlin, S.M., Littmann, E.R., Taur, Y., Sung, A.D., Weber, D., Hashimoto, D., Slingerland, A.E., Slingerland, J.B., et al. (2020). Microbiota as predictor of mortality in allogeneic hematopoietic-cell transplantation. N. Engl. J. Med. *382*, 822–834. https://doi.org/10.1056/NEJMoa1900623.
5. Caruso, R., Lo, B.C., and Núñez, G. (2020). Host-microbiota interactions in inflammatory bowel disease. Nat. Rev. Immunol. *20*, 411–426. https://doi.org/10.1038/s41577-019-0268-7.
6. Halfvarson, J., Brislawn, C.J., Lamendella, R., Vázquez-Baeza, Y., Walters, W.A., Bramer, L.M., D'Amato, M., Bonfiglio, F., McDonald, D., Gonzalez, A., et al. (2017). Dynamics of the human gut microbiome in

inflammatory bowel disease. Nat. Microbiol. *2*, 17004. https://doi.org/10.1038/nmicrobiol.2017.4.

7. Zeiser, R., and Blazar, B.R. (2017). Acute graft-versus-host disease - biologic process, prevention, and therapy. N. Engl. J. Med. *377*, 2167–2179. https://doi.org/10.1056/NEJMra1609337.
8. Bowerman, K.L., Varelias, A., Lachner, N., Kuns, R.D., Hill, G.R., and Hugenholtz, P. (2020). Continuous pre- and post-transplant exposure to a disease-associated gut microbiome promotes hyper-acute graft-versus-host disease in wild-type mice. Gut Microbes *11*, 754–770. https://doi.org/10.1080/19490976.2019.1705729.
9. Shono, Y., and van den Brink, M.R.M. (2018). Gut microbiota injury in allogeneic haematopoietic stem cell transplantation. Nat. Rev. Cancer *18*, 283–295. https://doi.org/10.1038/nrc.2018.10.
10. van Bekkum, D.W., Roodenburg, J., Heidt, P.J., and van der Waaij, D. (1974). Mitigation of secondary disease of allogeneic mouse radiation chimeras by modification of the intestinal microflora. J. Natl. Cancer Inst. *52*, 401–404. https://doi.org/10.1093/jnci/52.2.401.
11. Espey, M.G. (2013). Role of oxygen gradients in shaping redox relationships between the human intestine and its microbiota. Free Radic. Biol. Med. *55*, 130–140. https://doi.org/10.1016/j.freeradbiomed.2012.10.554.
12. Albenberg, L., Esipova, T.V., Judge, C.P., Bittinger, K., Chen, J., Laughlin, A., Grunberg, S., Baldassano, R.N., Lewis, J.D., Li, H., et al. (2014). Correlation between intraluminal oxygen gradient and radial partitioning of intestinal microbiota. Gastroenterology *147*. 1055–1063.e8. https://doi.org/10.1053/j.gastro.2014.07.020.
13. Donohoe, D.R., Garge, N., Zhang, X., Sun, W., O'Connell, T.M., Bunger, M.K., and Bultman, S.J. (2011). The microbiome and butyrate regulate energy metabolism and autophagy in the mammalian colon. Cell Metab. *13*, 517–526. https://doi.org/10.1016/j.cmet.2011.02.018.
14. Blouin, J.M., Penot, G., Collinet, M., Nacfer, M., Forest, C., Laurent-Puig, P., Coumoul, X., Barouki, R., Benelli, C., and Bortoli, S. (2011). Butyrate elicits a metabolic switch in human colon cancer cells by targeting the pyruvate dehydrogenase complex. Int. J. Cancer *128*, 2591–2601. https://doi.org/10.1002/ijc.25599.
15. Colgan, S.P., and Taylor, C.T. (2010). Hypoxia: an alarm signal during intestinal inflammation. Nat. Rev. Gastroenterol. Hepatol. *7*, 281–287. https://doi.org/10.1038/nrgastro.2010.39.
16. Mathewson, N.D., Jenq, R., Mathew, A.V., Koenigsknecht, M., Hanash, A., Toubai, T., Oravecz-Wilson, K., Wu, S.R., Sun, Y., Rossi, C., et al. (2016). Gut microbiome-derived metabolites modulate intestinal epithelial cell damage and mitigate graft-versus-host disease. Nat. Immunol. *17*, 505–513. https://doi.org/10.1038/ni.3400.
17. Fujiwara, H., Docampo, M.D., Riwes, M., Peltier, D., Toubai, T., Henig, I., Wu, S.J., Kim, S., Taylor, A., Brabbs, S., et al. (2018). Microbial metabolite sensor GPR43 controls severity of experimental GVHD. Nat. Commun. *9*, 3674. https://doi.org/10.1038/s41467-018-06048-w.
18. Kelly, C.J., Zheng, L., Campbell, E.L., Saeedi, B., Scholz, C.C., Bayless, A.J., Wilson, K.E., Glover, L.E., Kominsky, D.J., Magnuson, A., et al. (2015). Crosstalk between microbiota-derived short-chain fatty acids and intestinal epithelial HIF augments tissue barrier function. Cell Host Microbe *17*, 662–671. https://doi.org/10.1016/j.chom.2015.03.005.
19. Byndloss, M.X., and Bäumler, A.J. (2018). The germ-organ theory of non-communicable diseases. Nat. Rev. Microbiol. *16*, 103–110. https://doi.org/10.1038/nrmicro.2017.158.
20. Litvak, Y., Byndloss, M.X., Tsolis, R.M., and Bäumler, A.J. (2017). Dysbiotic Proteobacteria expansion: a microbial signature of epithelial dysfunction. Curr. Opin. Microbiol. *39*, 1–6. https://doi.org/10.1016/j.mib.2017.07.003.
21. Fujiwara, H., Seike, K., Brooks, M.D., Mathew, A.V., Kovalenko, I., Pal, A., Lee, H.J., Peltier, D., Kim, S., Liu, C., et al. (2021). Mitochondrial complex II in intestinal epithelial cells regulates T cell-mediated immunopathology. Nat. Immunol. *22*, 1440–1451. https://doi.org/10.1038/s41590-021-01048-3.
22. Stein-Thoeringer, C.K., Nichols, K.B., Lazrak, A., Docampo, M.D., Slingerland, A.E., Slingerland, J.B., Clurman, A.G., Armijo, G., Gomes, A.L.C., Shono, Y., et al. (2019). Lactose drives Enterococcus expansion to promote graft-versus-host disease. Science *366*, 1143–1149. https://doi.org/10.1126/science.aax3760.
23. Jenq, R.R., Ubeda, C., Taur, Y., Menezes, C.C., Khanin, R., Dudakov, J.A., Liu, C., West, M.L., Singer, N.V., Equinda, M.J., et al. (2012). Regulation of intestinal inflammation by microbiota following allogeneic bone marrow transplantation. J. Exp. Med. *209*, 903–911. https://doi.org/10.1084/jem.20112408.
24. Glover, L.E., Lee, J.S., and Colgan, S.P. (2016). Oxygen metabolism and barrier regulation in the intestinal mucosa. J. Clin. Invest. *126*, 3680–3688. https://doi.org/10.1172/JCI84429.
25. Ibrahim, A.S., Gebermariam, T., Fu, Y., Lin, L., Husseiny, M.I., French, S.W., Schwartz, J., Skory, C.D., Edwards, J.E., Jr., and Spellberg, B.J. (2007). The iron chelator deferasirox protects mice from mucormycosis through iron starvation. J. Clin. Invest. *117*, 2649–2657. https://doi.org/10.1172/JCI32338.
26. Packey, C.D., Shanahan, M.T., Manick, S., Bower, M.A., Ellermann, M., Tonkonogy, S.L., Carroll, I.M., and Sartor, R.B. (2013). Molecular detection of bacterial contamination in gnotobiotic rodent units. Gut Microbes *4*, 361–370. https://doi.org/10.4161/gmic.25824.
27. Toubai, T., Fujiwara, H., Rossi, C., Riwes, M., Tamaki, H., Zajac, C., Liu, C., Mathew, A.V., Byun, J., Oravecz-Wilson, K., et al. (2019). Host NLRP6 exacerbates graft-versus-host disease independent of gut microbial composition. Nat. Microbiol. *4*, 800–812. https://doi.org/10.1038/s41564-019-0373-1.
28. Song, X., Sun, X., Oh, S.F., Wu, M., Zhang, Y., Zheng, W., Geva-Zatorsky, N., Jupp, R., Mathis, D., Benoist, C., et al. (2020). Microbial bile acid metabolites modulate gut RORgamma(+) regulatory T cell homeostasis. Nature *577*, 410–415. https://doi.org/10.1038/s41586-019-1865-0.
29. Sato, Y., Atarashi, K., Plichta, D.R., Arai, Y., Sasajima, S., Kearney, S.M., Suda, W., Takeshita, K., Sasaki, T., Okamoto, S., et al. (2021). Novel bile acid biosynthetic pathways are enriched in the microbiome of centenarians. Nature *599*, 458–464. https://doi.org/10.1038/s41586-021-03832-5.
30. Campbell, C., McKenney, P.T., Konstantinovsky, D., Isaeva, O.I., Schizas, M., Verter, J., Mai, C., Jin, W.B., Guo, C.J., Violante, S., et al. (2020). Bacterial metabolism of bile acids promotes generation of peripheral regulatory T cells. Nature *581*, 475–479. https://doi.org/10.1038/s41586-020-2193-0.
31. Reddy, P., Sun, Y., Toubai, T., Duran-Struuck, R., Clouthier, S.G., Weisiger, E., Maeda, Y., Tawara, I., Krijanovski, O., Gatza, E., et al. (2008). Histone deacetylase inhibition modulates indoleamine 2,3-dioxygenase-dependent DC functions and regulates experimental graft-versus-host disease in mice. J. Clin. Invest. *118*, 2562–2573. https://doi.org/10.1172/JCI34712.
32. Toubai, T., Hou, G., Mathewson, N., Liu, C., Wang, Y., Oravecz-Wilson, K., Cummings, E., Rossi, C., Evers, R., Sun, Y., et al. (2014). Siglec-G-CD24 axis controls the severity of graft-versus-host disease in mice. Blood *123*, 3512–3523. https://doi.org/10.1182/blood-2013-12-545335.
33. Tamburini, F.B., Andermann, T.M., Tkachenko, E., Senchyna, F., Banaei, N., and Bhatt, A.S. (2018). Precision identification of diverse bloodstream pathogens in the gut microbiome. Nat. Med. *24*, 1809–1814. https://doi.org/10.1038/s41591-018-0202-8.
34. Semenza, G.L. (2012). Hypoxia-inducible factors in physiology and medicine. Cell *148*, 399–408. https://doi.org/10.1016/j.cell.2012.01.021.
35. Karhausen, J., Furuta, G.T., Tomaszewski, J.E., Johnson, R.S., Colgan, S.P., and Haase, V.H. (2004). Epithelial hypoxia-inducible factor-1 is protective in murine experimental colitis. J. Clin. Invest. *114*, 1098–1106. https://doi.org/10.1172/JCI21086.
36. Shah, Y.M., Ito, S., Morimura, K., Chen, C., Yim, S.H., Haase, V.H., and Gonzalez, F.J. (2008). Hypoxia-inducible factor augments experimental colitis through an MIF-dependent inflammatory signaling cascade. Gastroenterology *134*. e2031–e2033. https://doi.org/10.1053/j.gastro.2008.03.009.

37. Xu, M., Tao, J., Yang, Y., Tan, S., Liu, H., Jiang, J., Zheng, F., and Wu, B. (2020). Ferroptosis involves in intestinal epithelial cell death in ulcerative colitis. Cell Death Dis. *11*, 86. https://doi.org/10.1038/s41419-020-2299-1.

38. Xu, S., He, Y., Lin, L., Chen, P., Chen, M., and Zhang, S. (2021). The emerging role of ferroptosis in intestinal disease. Cell Death Dis. *12*, 289. https://doi.org/10.1038/s41419-021-03559-1.

39. Ellermann, M., and Arthur, J.C. (2017). Siderophore-mediated iron acquisition and modulation of host-bacterial interactions. Free Radic. Biol. Med. *105*, 68–78. https://doi.org/10.1016/j.freeradbiomed.2016.10.489.

40. Schloss, P.D., Westcott, S.L., Ryabin, T., Hall, J.R., Hartmann, M., Hollister, E.B., Lesniewski, R.A., Oakley, B.B., Parks, D.H., Robinson, C.J., et al. (2009). Introducing Mothur: open-source, platform-independent, community-supported software for describing and comparing microbial communities. Appl. Environ. Microbiol. *75*, 7537–7541. https://doi.org/10.1128/AEM.01541-09.

41. Segata, N., Izard, J., Waldron, L., Gevers, D., Miropolsky, L., Garrett, W.S., and Huttenhower, C. (2011). Metagenomic biomarker discovery and explanation. Genome Biol. *12*, R60. https://doi.org/10.1186/gb-2011-12-6-r60.

42. Schindelin, J., Arganda-Carreras, I., Frise, E., Kaynig, V., Longair, M., Pietzsch, T., Preibisch, S., Rueden, C., Saalfeld, S., Schmid, B., et al. (2012). Fiji: an open-source platform for biological-image analysis. Nat. Methods *9*, 676–682. https://doi.org/10.1038/nmeth.2019.

43. Wickham, H. (2016). Elegant Graphics for Data Analysis. Use R!, Second Edition (Springer International Publishing), p. ggplot2.

44. Shah, Y.M., Matsubara, T., Ito, S., Yim, S.H., and Gonzalez, F.J. (2009). Intestinal hypoxia-inducible transcription factors are essential for iron absorption following iron deficiency. Cell Metab. *9*, 152–164. https://doi.org/10.1016/j.cmet.2008.12.012.

45. Cooke, K.R., Hill, G.R., Crawford, J.M., Bungard, D., Brinson, Y.S., Delmonte, J., Jr., and Ferrara, J.L. (1998). Tumor necrosis factor- alpha production to lipopolysaccharide stimulation by donor cells predicts the severity of experimental acute graft-versus-host disease. J. Clin. Invest. *102*, 1882–1891. https://doi.org/10.1172/JCI4285.

46. Hill, G.R., Cooke, K.R., Teshima, T., Crawford, J.M., Keith, J.C., Jr., Brinson, Y.S., Bungard, D., and Ferrara, J.L. (1998). Interleukin-11 promotes T cell polarization and prevents acute graft-versus-host disease after allogeneic bone marrow transplantation. J. Clin. Invest. *102*, 115–123. https://doi.org/10.1172/JCI3132.

47. Kozich, J.J., Westcott, S.L., Baxter, N.T., Highlander, S.K., and Schloss, P.D. (2013). Development of a dual-index sequencing strategy and curation pipeline for analyzing amplicon sequence data on the MiSeq Illumina sequencing platform. Appl. Environ. Microbiol. *79*, 5112–5120. https://doi.org/10.1128/AEM.01043-13.

48. Koenigsknecht, M.J., Theriot, C.M., Bergin, I.L., Schumacher, C.A., Schloss, P.D., and Young, V.B. (2015). Dynamics and establishment of Clostridium difficile infection in the murine gastrointestinal tract. Infect. Immun. *83*, 934–941. https://doi.org/10.1128/IAI.02768-14.

49. Wang, Q., Garrity, G.M., Tiedje, J.M., and Cole, J.R. (2007). Naive Bayesian classifier for rapid assignment of rRNA sequences into the new bacterial taxonomy. Appl. Environ. Microbiol. *73*, 5261–5267. https://doi.org/10.1128/AEM.00062-07.

50. Cole, J.R., Wang, Q., Fish, J.A., Chai, B., McGarrell, D.M., Sun, Y., Brown, C.T., Porras-Alfaro, A., Kuske, C.R., and Tiedje, J.M. (2014). Ribosomal Database Project: data and tools for high throughput rRNA analysis. Nucleic Acids Res. *42*, D633–D642. https://doi.org/10.1093/nar/gkt1244.

51. Campbell, E.L., Bruyninckx, W.J., Kelly, C.J., Glover, L.E., McNamee, E.N., Bowers, B.E., Bayless, A.J., Scully, M., Saeedi, B.J., Golden-Mason, L., et al. (2014). Transmigrating neutrophils shape the mucosal microenvironment through localized oxygen depletion to influence resolution of inflammation. Immunity *40*, 66–77. https://doi.org/10.1016/j.immuni.2013.11.020.

52. Kim, Y.G., Sakamoto, K., Seo, S.U., Pickard, J.M., Gillilland, M.G., 3rd, Pudlo, N.A., Hoostal, M., Li, X., Wang, T.D., Feehley, T., et al. (2017). Neonatal acquisition of Clostridia species protects against colonization by bacterial pathogens. Science *356*, 315–319. https://doi.org/10.1126/science.aag2029.

STAR★METHODS

KEY RESOURCES TABLE

REAGENT or RESOURCE	SOURCE	IDENTIFIER
Antibodies		
CD90.2 MicroBeads, mouse	Miltenyi Biotec	Cat# 130-121-278
CD5 (Ly-1) MicroBeads, mouse	Miltenyi Biotec	Cat# 130-049-301
DAPI	BioLegend	Cat# 422801
Rat Anti-Mouse CD4 Antibody, APC-H7 Conjugated	BD Biosciences	Cat# 560246, RRID:AB_1645236
APC anti-mouse CD25	BioLegend	Cat# 101910, RRID: AB_2280288
FITC anti-mouse/human CD44 antibody	BioLegend	Cat# 103006, RRID:AB_312957
PE anti-mouse CD45RB antibody	BioLegend	Cat# 103308, RRID:AB_313015
FITC anti-mouse CD8a antibody	BioLegend	Cat# 100705, RRID:AB_312744
FITC anti-mouse IL-17A antibody	BioLegend	Cat# 506907, RRID:AB_536009
FITC anti-mouse CD25 antibody	BioLegend	Cat# 101907, RRID:AB_961210
FITC anti-mouse CD11c antibody	BioLegend	Cat# 117305, RRID:AB_313774
FITC anti-mouse CD80 antibody	BioLegend	Cat# 104705, RRID:AB_313126
PE anti-mouse CD62L antibody	BioLegend	Cat# 104407, RRID:AB_313094
PE anti-mouse CD69 antibody	BioLegend	Cat# 104507, RRID:AB_313110
PE anti-mouse IFN-gamma antibody	BioLegend	Cat# 505807, RRID:AB_315401
PE anti-mouse FOXP3 antibody	BioLegend	Cat# 126403, RRID:AB_1089118
Rat Anti-CD40 Monoclonal Antibody, Phycoerythrin Conjugated, Clone 3/23	BD Biosciences	Cat# 553791, RRID:AB_395055
PE anti-mouse CD274 (B7-H1, PD-L1) antibody	BioLegend	Cat# 124307, RRID:AB_2073557
PE anti-mouse IL-6 antibody	BioLegend	Cat# 504503, RRID:AB_315337
PerCP/Cyanine5.5 anti-mouse CD45.2 antibody	BioLegend	Cat# 109827, RRID:AB_893352
APC anti-mouse/human CD44 antibody	BioLegend	Cat# 103011, RRID:AB_312962
APC anti-mouse CD279 (PD-1) antibody	BioLegend	Cat# 135209, RRID:AB_2251944
APC anti-mouse IL-4 antibody	BioLegend	Cat# 504105, RRID:AB_315319
ROR gamma (t) Monoclonal Antibody (AFKJS-9), APC,	Thermo Fisher Scientific	Cat# 17-6988-82, RRID:AB_10609207
APC anti-mouse CD11c antibody	BioLegend	Cat# 117309, RRID:AB_313778
APC anti-mouse TNF-alpha antibody	BioLegend	Cat# 506307, RRID:AB_315428
APC/Cyanine7 anti-mouse CD4 antibody	BioLegend	Cat# 100413, RRID:AB_312698
HIF1A-human antibody	GeneTex	Cat# GTX127309, RRID:AB_2616089)
HIF Prolyl Hydroxylase 3 Antibody	Novus Biologicals	Cat# NB100-139, RRID:AB_2096716
Mouse Anti-Actin, beta Monoclonal Antibody, Unconjugated, Clone mAbcam 8226	Abcam	Cat# ab8226, RRID:AB_306371
Anti-rabbit IgG, HRP-linked Antibody	Cell Signaling Technology	Cat# 7074, RRID:AB_2099233
HIF-1 alpha Antibody	Novus Biologicals	Cat# NB100-479, RRID:AB_10000633
Goat Anti-Rabbit IgG H&L (HRP polymer)	abcam	Cat# ab214880
Chemicals, peptides, and recombinant proteins		
Ampicillin	Sigma Aldrich	Cat# A9393
Kanamycin sulfate	Sigma Aldrich	Cat# 60615
Metronidazole	Sigma Aldrich	Cat# M1547
Vancomycin	Sigma Aldrich	Cat# SBR00001
Neomycin	Sigma Aldrich	Cat# N1876
Deferasirox	Sigma Aldrich	Cat# SML2673-50
HBSS (10X), no calcium, no magnesium, no phenol red	Gibco	Cat# 14185052

(*Continued on next page*)

Continued

REAGENT or RESOURCE	SOURCE	IDENTIFIER
Sodium bicarbonate	Sigma Aldrich	Cat# S6014
FBS	GeminiBio	Cat# 100-106
0.5 M EDTA Solution	Lonza	Cat# 51201
Red blood cell lysing buffer	Sigma Aldrich	Cat# R7757
DTT	Gold Biotechnology	Cat# DTT
Percoll PLUS	GE Healthcare	Cat# 17-5445
PMA	Sigma Aldrich	Cat# P1585
Ionomycin	Sigma Aldrich	Cat# I3909
LPS	Sigma Aldrich	Cat# L2654
Protein Transport Inhibitor Cocktail	eBioscience	Cat# 00-4980-03
IC Fixation Buffer	eBioscience	Cat# 00-8222-49
Permeabilization Buffer (10X)	eBioscience	Cat# 00-8333-56
RIPA Lysis and Extraction Buffer	Thermo Scientific	Cat# 89901
ECL Western Blotting Substrate	Thermo Scientific	Cat# 32106
Goat Serum, New Zealand origin	Gibco	Cat# 16210064
ImmPACT® DAB Substrate Kit, Peroxidase (HRP)	VECTOR labolatories	Cat# SK-4105
ProLong™ Gold Antifade Mountant with DAPI	Invitrogen	Cat# P36931
Seahorse XF Media	Agilent	Cat# 102353-100
D-(+)-Glucose	Sigma Aldrich	Cat# G7021
FCCP	abcam	Cat# ab120081
Oligomycin A	Sigma Aldrich	Cat# 75351
Rotenone	Tocris	Cat# 3616
Antimycin A from Streptomyces sp.	Sigma Aldrich	Cat# A8674
Critical commercial assays		
MagAttract PowerMicrobiome DNA/RNA EP	QIAGEN	Cat# 27500-4-EP
Quant-iT™ PicoGreen™ dsDNA Assay Kits and dsDNA Reagents	Invitrogen	Cat# P7589
MiSeq Reagent Kits v2	illumina	Cat# MS-102-2003
NuPAGE™ 4 to 12%, Bis-Tris, 1.0–1.5 mm, Mini Protein Gels	Invitrogen	Cat# NP0321BOX
Immobilon®-PSQ Membrane, PVDF, 0.2 m, 8.5 cm x 10 m roll	Millipore	Cat# ISEQ85R
Hypoxyprobe-Red549 Kit	Hypoxyprobe	Cat# HP7
RNeasy Micro Kit	QIAGEN	Cat# 74004
High-Capacity cDNA Reverse Transcription Kit with RNase Inhibitor	Applied Biosystems	Cat# 4374966
Iron Assay Kit	Sigma Aldrich	Cat# MAK025
Deposited data		
Code used for analysis for 16S rRNA sequencing: https://doi.org/10.5281/zenodo.7401507.	zenodo	https://doi.org/10.5281/zenodo.7401507.
Experimental models: Organisms/strains		
Mouse: C57BL/6	Charles River Laboratories	Cat# 027, RRID:IMSR_CRL:027
Mouse: BALB/c	Charles River Laboratories	Cat# 028, RRID:IMSR_CRL:028
Mouse: BDF1	Charles River Laboratories	Cat# 099, RRID:IMSR_CRL:099
Mouse: B6.129S7-Rag1^{tm1Mom}/J	The Jackson Laboratories	Cat# 002216, RRID:IMSR_JAX:002216
Mouse: BDF1	The Jackson Laboratories	Cat# 100006, RRID:IMSR_JAX:100006
Mouse: B6.Cg-Tg(Vil1-cre)1000Gum/J	The Jackson Laboratories	Cat# 021504, RRID:IMSR_JAX:021504
Mouse: 129S1/SvImJ	The Jackson Laboratories	Cat# 002448, RRID:IMSR_JAX:002448
Mouse: C57BL/6NTac	Taconic Biosciences	Cat# B6 F, RRID:IMSR_TAC:b6
Mouse: BALB/cAnNTac	Taconic Biosciences	Cat# BALB-F, RRID:IMSR_TAC:balb

(*Continued on next page*)

Continued

REAGENT or RESOURCE	SOURCE	IDENTIFIER
Mouse: Hif1a$^{fl/fl}$	Gift from Yatrik M. Shah	N/A
Oligonucleotides		
RNA sequence, mouse *Gapdh*: 5′-TGACCTCAACTACATGGTCTACA-3′ and 5′-CTTCCCATTCTCGGCCTTG-3′	This paper	N/A
RNA sequence, mouse *Hif1α*: 5′-CAGTCACCTGGTTGCTGCAA -3′ and 5′-CAGTCACCTGGTTGCTGCAA -3′	This paper	N/A
RNA sequence, mouse *Egln(Phd3)*: 5′-TGCTGAAGAAAGGGCAGAAG -3′ and 5′-GCACACCACAGTCAGTCTTTA-3′	This paper	N/A
Software and algorithms		
FlowJo	BD	https://www.flowjo.com, RRID:SCR_008520, version 10.2
mothur	Schloss et al.[40]	https://mothur.org/, RRID:SCR_011947, version 1.40.2 and 1.42.3
LEfSe	Segata et al.[41]	http://huttenhower.sph.harvard.edu/galaxy, RRID:SCR_014609, version 1.1.2
ggpubr	https://cloud.r-project.org/web/packages/ggpubr/index.html	https://CRAN.R-project.org/package=ggpubr, RRID:SCR_021139, version 0.4.0
ggplot2	Wickham[42]	https://cran.r-project.org/web/packages/ggplot2/index.html, RRID:SCR_014601version 3.3.5
R	R Foundation	http://www.r-project.org/, RRID:SCR_001905, version 4.1.3
ImageJ	Schindelin et al.[43]	https://imagej.net/software/fiji/, RRID:SCR_003070, version 1.53c
Seahorse Wave Desktop Software	Agilent	https://www.agilent.com/en/products/cell-analysis/software-download-for-wave-desktop, RRID:SCR_014526, version 2.6.1.53
Graph Pad Prism	Graph Pad Software Inc	http://www.graphpad.com/, RRID:SCR_002798, version 8.0.0,
Excel2016	Microsoft	https://www.microsoft.com/en-us/microsoft-365/excel, RRID:SCR_016137, version 2105

RESOURCE AVAILABILITY

Lead contact

Further information and requests for resources and reagents should be directed to and will be fulfilled by the lead contact, Reddy Pavan (Pavan.Reddy@bcm.edu).

Materials availability

This study did not generate new unique reagents.

Data and code availability

Unprocessed 16s rRNA sequencing reads were deposited at the NCBI Short Read Archive (SRA) and are accessible via BioProject PRJNA910578.

The code used for analysis for 16S rRNA sequencing is available at https://doi.org/10.5281/zenodo.7401507.

Any additional information required to reanalyze the data reported in this paper is available from the lead contact upon request.

EXPERIMENTAL MODEL AND SUBJECT DETAILS

Mice

C57BL/6 (027, B6, H-2K^{b}, CD4+5.2), BALB/c (028, H-2K^{d}), and BDF1 (099, H-2K$^{b/d}$) were purchased from Charles River Laboratories. B6.129S7-Rag1^{tm1Mom}/J(002216, Rag1$^{-/-}$) mice, BDF1 (100006, B6D2F1/J), B6.Cg-Tg(Vil1cre)1000Gum/J mice(021504),

and 129 (002448, 129S1/SvImJ) were purchased from the Jackson Laboratory. Taconic B6 (B6-F, C57BL/6NTac) and Taconic BALB/c (BALB-F, BALB/cAnNTac) were purchased from Taconic. Hif1a-floxed mice (Hif1a$^{fl/fl}$, C57BL/6 background)[44] containing the loxP site were crossed with Vil1cre mice (C57BL/6 background) to generate intestinal epithelial cells specific HIF1a-null mice (Hif1a$^{fl/fl}$ Vil1-cre mice). Germ free (GF) C57BL/6 mice and Rag1$^{-/-}$ GF mice were raised and housed in ISOcage Positive isolators (Techniplast) at the germ-free mouse facility at the University of Michigan. Germ-free status was verified by aerobic, anaerobic cultures, and gram stain. 6-12 weeks old female mice used for experiments. All mice were kept under specific pathogen-free (SPF) conditions or GF conditions and cared for according to regulations reviewed and approved by the University of Michigan Committee on the Use and Care of Animals (PRO00009494), which are based on the University of Michigan Laboratory Animal Medicine guidelines. Mouse studies from MSKCC followed the respective Institutional Animal Care and Use Committee guidelines (99-07-025) and were kept under specific pathogen-free (SPF) conditions. B6 mice 6-8 weeks old were treated with 2 weeks of antibiotics cocktail (ampicillin 1mg/ml (A9393, Sigma Aldrich) + kanamycin 1mg/l (60615, Sigma Aldrich) + metronidazole 1mg/ml (M1547, Sigma Aldrich) + vancomycin 0.5mg/l (SBR00001, Sigma Aldrich) plus 3% stevia or ampicillin 1 mg/ml + neomycin 1mg/ml + metronidazole 1mg/ml + vancomycin 0.5mg/ml in filtered double distillated drinking water. BMT recipients were orally treated with deferasirox (20mg/kg, SML2673-50, Sigma Aldrich) and vehicle every day until day21 after BMT. For the co-housing experiments, mice were co-housed in a ratio of 1:1 naïve mice, B6 Ab, and BMT mice respectively. For Figure 1A, Allo B6 and B6 were co-housed. For Figure 1G, SynB6 or Allo B6 were co-housed with B6Ab. For Figure 3A, the design of the experiment is same as Figure 1A. For the fecal microbiota transplant, mice were gavaged by 10 doses of intestinal content from recipient mice for 2weeks. Each gavage day one BMT mouse whole intestinal content was collected and homogenized in sterile PBS. 200ul of the solution was gavaged to each recipient mouse.

Hematopoietic cell transplantation model

Transplantations were performed as previously described.[31] Briefly, Splenic T cells from donors were enriched, and T-cell-depleted BM (TCD-BM) was depleted of T cells by autoMACS (Miltenyi Biotec) utilizing CD90.2 microbeads (130-121-278, Miltenyi Biotec) or CD5 microbeads (130-049-301, Miltenyi Biotec). The details of HCT model were described in Table S1. The mice were randomly assigned to syngeneic, allogeneic or treatment groups in each experiment.

Colitis models

For the T-cell transfer induced colitis model, isolated splenic T cells from B6 mice were stained with DAPI (#422801, 1μM, Biolenged), APC-Cy7 anti-CD4+ (560246, GK1.5, 1:100, BD Biosciences, San Jose, CA), APC anti-CD25 (101910, 3C7, 1:100, Biolegend), FITC anti-CD4+4 (103006, IM7, 1:100, Biolegend) and PE anti-CD4+5RB (103308, C363-16A, 1:100, Biolegend). CD4+$^{+}$CD25^{-}CD4+4^{-}CD4+5RB^{hi} cells were sorted with the MoFlo Astrios cell sorter (Beckman Coulter) and intraperitoneally injected into *Rag-1*$^{-/-}$ SPF or GF recipients.

METHOD DETAILS

Systemic and histopathological analysis of GVHD

Survival after HCT was monitored daily and assessed the degree of clinical GVHD weekly, as described in Table S2.[45] Histopathological analysis of the liver, gastrointestinal (GI) tract, and lung, which are the primary GVHD target organs, was performed as described utilizing a semi-quantitative scoring system implemented in a blinded manner by a single pathologist (C.L.).[46] A pathology scoring of GVHD was used to assess the following abnormalities known to be associated with GVHD. Small intestine: villous blunting, crypt regeneration, loss of enterocyte brush border, luminal sloughing of cellular debri, crypt cell apoptosis, outright crypt destruction, and lamina propria lymphocytic infiltrate; colon: crypt regeneration, surface coloncytes, colonocyte vacuolization, surface colonocyte attenuation, crypt cell apoptosis, outright crypt destruction, and lamina propria lymphocytic infiltrate. The scoring system denoted 0 as normal, 0.5 as focal and rare, 1.0 as focal and mild, 2.0 as diffuse and mild, 3.0 as diffuse and moderate, and 4.0 as diffuse and severe. Scores were added to provide a total score for each specimen. Only after scoring was performed were codes broken and data compiled. After scoring, the codes were broken, and the data compiled.

DNA extraction, 16S rRNA gene sequencing and data analysis

The University of Michigan Microbiome Core extracted DNA and prepared and sequenced the amplicon libraries. DNA was extracted using an Eppendorf EpMotion liquid handling system and the Qiagen MagAttract PowerMicrobiome kit (previously MoBio PowerMag Microbiome, 27500-4-EP, Qiagen) kit and protocol. DNA (1 μl) was quantified with the Quant-iT PicoGreen dsDNA Assay kit (p7589, Invitrogen).

The University of Michigan Microbiome Core prepared and sequenced the amplicon libraries. Extracted DNA was amplified with dual-index primers targeting the V4 region of the 16S rRNA gene, as previously described[47] with the following PCR conditions: 2 min at 95°C, 30 cycles x [95°C for 20 s, 55°C for 15 s, and 72°C for 5 min], followed by 72°C for 10 min. Libraries were prepared as previously described,[48] with minor modifications: the final library concentration was 5.5 pM and 15% PhiX spike-in was added to increase diversity. Sequencing was performed on an Illumina MiSeq using the 500 cycles MiSeq Reagent Kit V2 (catalog no. MS-102-2003) with modifications described in the Schloss MiSeq SOP.[47]

Paired-end 16S V4 sequences were processed using the software Mothur[40] (version 1.40.2 for first sequencing run, version 1.42.3 for subsequent run). The Schloss MiSeq SOP[47] as of August 2019 was followed to reduce PCR and sequencing errors. The sequences were aligned to a reference alignment based on SILVA release 132. After pre-clustering and chimera removal with vsearch, the remaining sequences (as well as the OTUs later) were classified to RDP taxonomy[49] based on RDP training set no 16.[50] The bacterial 16S V4 sequences were phylotyped into genus bins to make community composition bar plots and clustered into 97% identity OTUs, with OTU abundance compiled for subsequent statistical analysis. These steps also followed the Schloss MiSeq SOP. Based on OTU abundance, PCoA was plotted and alpha diversity estimated with inverse Simpson. Differentially abundant taxa were determined with LEfSe version 1.1.2[41]; cladograms and LDA scores of LEfSe results were plotted using the same software.

The relative abundance of bacterial OTUs grouped by oxygen sensitivity were compared by summing the relative abundance of known obligate anaerobes (Actinomyces, Bacteroides, Clostridium, Faecalibacterium, Blautia, Ruminococcus, Parabacteroides, and Bifidobacterium), facultative anaerobes (Escherichia/Shigella, Klebsiella, Salmonella, Enterococcus, Lactobacillus, and Staphylococcus), and unclassified. Differences in relative abundance between experimental groups were evaluated with Wilcoxon signed-rank tests using the ggpubr (version 0.4.0) and ggplot2[43] (version 3.3.5) R packages in R version 4.1.3. Unprocessed 16s rRNA sequencing reads were deposited at the NCBI Short Read Archive (SRA) and are accessible via BioProject PRJNA910578. The code used for analysis for 16S rRNA sequencing is available at https://doi.org/10.5281/zenodo.7401507.

Intestinal epithelial cells and intraepithelial cells isolation

Luminal contents from dissected colon and ileum were flushed with CMF buffer; Ca^{2+}/Mg^{2+} free HBSS (14185052, Thermo Fisher Scientific) supplemented with 25mM sodium bicarbonate (S6014, Sigma-Aldrich) and 2% FBS (100-106, Gemini Bio Products, USA). Intestines were then minced into 5mm pieces, washed with CMF buffer four times, transferred to CMF with 5mM EDTA (51201, Lonza), and incubated at 37 °C for 40 minutes (shaking tubes every 10 minutes). Supernatants containing IECs were then transferred through 100 μM cell filter followed by incubation on ice for 10 minutes to allow sedimentation. Supernatants were again transferred through a 75 μM cell filter.

Preparation of lymphocytes single cell suspension and flow cytometry

Systemic lymph nodes (axillary and inguinal), mesenteric lymph nodes and spleens were mechanically disrupted. Red blood cells were lysed (R7757, Sigma-Aldrich). For intra epithelial lymphocytes (IEL) isolation, intestines were minced in HBSS buffer (141850, Gibco) supplemented with 2.5% heat-inactivated FBS (100-106, Gibco) (HBSS+) and washed with magnetic stirring at 37°C. Intestine pieces were then incubated in HBSS+/1 mM DTT (DTT, Gold Biotechnology) at 37°C followed by additional washes and incubation in HBSS+/1mM EDTA (51201, Lonza). The supernatant was then layered on a 75%/40% Percoll Plus (17-5445, GE Healthcare) gradient to collect enriched IELs.

Single cell suspensions were resuspended in FACS wash buffer (2% bovine serum albumin in PBS). Cells were stained with conjugated monoclonal antibodies (mAbs): fluorescein isothiocyanate (FITC)–conjugated mAbs to CD8+ (100705, clone 53-6.7, BioLegend), IL-17A (506907, clone TC11-18H10.1, BioLegend), CD25 (101907, clone 3c7, BioLegend), CD11c (117305, clone N418, BioLegend) and CD8+0 (104705, clone 16-10A1, Biolegend); phycoerythrin (PE)-conjugated mAbs to CD62L (104407, clone MEL-14, BioLegend), CD69 (104507, clone H1.2F3, BioLegend), IFNγ (505807, clone XMG1.2,BioLegend), FoxP3 (126403, clone MF-14, BioLegend), CD4+0 (553791, clone 3/23, BD Pharmingen), CD274 (124307, PD-L1, clone 10F.9G2, BioLegend), IL-6 (504503, clone MP5-20F3, BioLegend); PerCP-Cy5.5 to CD4+5.2 (109827, clone 104, BioLegend); APC-conjugated mAbs to mouse CD4+4 (103011, clone IM7, BioLegend), CD279 (PD-1, 135209, clone 29F.1.A12, BioLegend), IL4 (504105, clone 11B11, BioLegend), RORγt (17-6988-82, clone AFKJS-9, Invitrogen), CD11c (117309, clone N418, BioLegend), TNFα (506307, clone MP6-XT22, BioLegend); and APC-Cy7 to CD4+ (100413, clone GK1.5, BioLegend). For cytokine analysis, cells were treated with RPMI containing 10% FBS, phorbol 12-myr-istate 13-acetate (PMA) (10 ng/mL, P1585, Sigma-Aldrich)/Ionomycin (1mM, I3909, Sigma-Aldrich) cocktail or lipopolysaccharide (LPS, 500ng/mL, L2654, Sigma-Aldrich) in the presence of protein transport inhibitor cocktail (X500, 00-4980-03, eBioscience) at 37°C for 6 hours. For intracellular staining, cells were fixed with FoxP3 staining buffer set (FoxP3 and RORγt) or IC fixation buffer (for cytokines, 00-8222-49, eBioscience) and permeabilized with permeabilization buffer (00-8333-56, eBioscience) according to the manufacturer protocol. Cells were analyzed using the Attune NxT flow cytometer.

Immunoblot analysis

Isolated mitochondria or IECs were lysed in RIPA buffer (89901, Thermo Scientific). Equal amounts of proteins were loaded on 4-12% SDS-PAGE gel (NP0321, Invitrogen), electrophoresed and subsequently transferred to a PVDF membrane (ISEQ85R, Millipore) using a Bio-Rad semi-dry transfer cell (20 V, 1 h). Blots were incubated with anti-HIF1a (GTX127309, polyclonal, 1:1000, GeneTex), anti-PHD3 (NB100-139, 1:1000, Novus Biologicals), and anti-β actin (8226, mAbcam8226, 1:3000, Abcam) primary antibodies overnight at 4°C. Incubation with secondary anti-rabbit-HRP (7074S, Cell Signaling Technology) was performed at room temperature for 1 hour. Bound antibody was detected using Super Signal ECL substrate (32106, Thermo Scientific) and quantitated using ChemiDoc MP Imaging system (BioRad). Densitometric analysis was performed using Image J[42] (v 1.53c).

Immunohistochemistry staining

For Hif1α staining, colonic tissues were processed, embedded in paraffin, and cut into 5 μm sections. Slides were de-paraffinized, and heat-induced antigen retrieval was performed with 10 mM sodium citrate buffer. Endogenous peroxidases were quenched with

3.0% hydrogen peroxide for 15 min. Primary anti-Hif1 α (NB100-479, Novus Biologicals) was diluted 1:200 in PBST containing 10% goat serum (16210064, Thermo Fisher Scientific) and incubated for 60 min at room temperature. Bound anti-body was detected using an anti-rabbit HRP labeled polymer (ab214880, abcam) incubated for 30 min and ImmPACT DAB (SK-4105, VECTOR labolatories). Slides were then counterstained with hematoxylin, dehydrated, and covered. For hypoxia staining, recipient mice were administered pimonidazole (PMDZ, HP7) from Hypoxyprobe, Inc. by intraperitoneal injection 30 min prior to sacrifice. Colon and ileum samples were paraffin-embedded and stained according to the manufacturer's instructions and counterstained with DAPI (P36931, Thermo Scientific).[51]

Seahorse analysis

IECs were resuspended with complete seahorse XF assay medium (103335-100, Aglient) with 17.5 mM glucose (G7021, Sigma-Aldrich), 1 mM sodium pyruvate (S8636, Sigma-Aldrich), 2 mM glutamine (GLL02, Caisson Labs), 2 %BSA (BP1600-100, Fisher Scientific), 10uM Y-27632 and 1% penicillin-streptomycin (516106, Sigma-Aldrich) adjusted to pH 7.4. Cells were plated at 8×10^4 cells per well in a Seahorse assay plate, pretreated with matrigel (354262, Corning). Cells were equilibrated to 37 °C for 30 min before assay. Respiration profile was assessed in 96XF instrument with Mitostress assay as indicated upon cell treatment with 5 μM FCCP (ab120081, abcam), 7.5μM oligomycin A (75351, Sigma-Aldrich), 4μM Rotenone (3616, Tocris), and 4μM antimycin A (A8674, Sigma-Aldrich). Seahorse Wave Desktop Software (version 2.6.1.53) was used for data analysis.

Measurements of oxygen concentration in colonic mucosa

C57BL/6 mice post HCT day7 and day 21 were subject to be determined oxygen concentration levels in the colonic mucosa. The oxygen Pst1 optode microsensors (Presens) at the tip of a fiber optic cable were used. The optode was inserted into the mouse's colon at a depth of one to three cm via an endoscope (Karl Storz). Before oxygen measurements, mice were anesthetized with 4% isoflurane and then received 2% isoflurane during the oxygen measurement. The colon was insufflated with nitrogen gas to expunge both extraneous oxygen and oxygen that had leached into the rectum when insertion of the endoscope. Visual assessments of when the microsensor contacted with the colonic mucosa using a camera attached to the endoscope. Oxygen concentrations were recorded with a PreSens Microx TX3 Trace Micro fiber optic O2 transmitter and Presens' Oxyview TX3 v. 5.31 software using default parameters. Prior to measurements, a two-point calibration of the microsensor was conducted with air-saturated water and 100 ml of anoxic water that was attained by the addition of one gram of sodium sulfite (Acros Organics) and 50 μL of 500 mM cobalt nitrate solution (Acros Organics). Mouse body was kept on a 37°C heating pad with a Gaymar T-pump system. To prepare the colon for imaging, the colon was flushed with water. Oxygen concentration readings from the mucosa that remained stable for at least 30 seconds were recorded. Readings from three to five locations in the colon were then obtained for each mouse; readings from each location were subsequently averaged to obtain a mean oxygen concentration for each mouse.[52]

RNA isolation and RT-PCR

RNA isolation and RT-PCR: Total RNA from single-cell suspensions was isolated using the RNeasy Kit (74104, QIAGEN) and reverse transcribed into cDNA using the High Capacity cDNA Reverse Transcription Kit (4374966, Applied Biosystems). The following primers and PowerUP SYBR green polymerase were used to detect the following transcripts:; 5′-TGACCTCAACTACATGGTC TACA-3′ and 5′-CTTCCCATTCTCGGCCTTG-3′ (*Gapdh*), 5′-CAGTCACCTGGTTGCTGCAA -3′ and 5′-CAGTCACCTGGTTGCTG CAA -3′ (*Hif1α*), 5′-TGCTGAAGAAAGGGCAGAAG -3′ and 5′-GCACACCACAGTCAGTCTTTA-3′ (*Egln: Phd3*). All reactions were performed according to manufacturer's instructions. All primers were verified for the production of a single specific PCR product via melting curve analysis

Quantification of iron in intestinal content

The intestinal content in colon and ileum from allogeneic recipient mice were collected after euthanized. Then, the intestinal contents were processed according to the manufacturer's instruction of Iron Assay Kit (MAK025, Sigma-Aldrich).

QUANTIFICATION AND STATISTICAL ANALYSIS

All statistical analysis was performed using Graph Pad Prism (v8.0.0, Graph Pad Software Inc) and Excel2016 (version2105) to do the graph figures and statistics. P values <0.05 were considered as significant: P values >0.05 were considered as non-significant (* $p<0.05$, ** $p<0.01$, *** $p<0.001$ and **** $p<0.0001$). All sample sizes and statistical tests used are detailed in each figure legend. All replicates are biological replicates. No data were excluded. All experiments in vitro and in vivo were performed twice or more than twice. Data shown as ±SEM according to figure legend.